TECHNISCHE UNIVERSITÄT WIEN

DIPLOMA THESIS

Thermochemical energy storage

Experimental investigation of innovative material systems for the suspension reactor

carried out for the purpose of obtaining the degree of Master of Science,

submitted at

Institute of Chemical, Environmental and Bioscience Engineering

Faculty of Technical Chemistry

Technischen Universität Wien

under the supervision of

Univ.-Prof. Dipl.-Ing. Dr. techn. Franz Winter

Dipl.-Ing. Lena Schmieder, BSc.

by

Sarah Wimmer BSc.

Mat.Nr.: 11715008

Vienna, 26.03.2023

[redacted]

(Signature)

I confirm, that going to press of this thesis under the term

Master thesis

needs the confirmation of the examination committee.

Affidavit

I declare in lieu of oath, that I wrote this thesis and performed the associated research myself, using only literature cited in this volume. If text passages from sources are used literally, they are marked as such.

I confirm that this work is original and has not been submitted elsewhere for any examination, nor is it currently under consideration for a thesis elsewhere.

I acknowledge that the submitted work will be checked electronically-technically using suitable and state-of-the-art means (plagiarism detection software). On the one hand, this ensures that the submitted work was prepared according to the high-quality standards within the applicable rules to ensure good scientific practice "Code of Conduct" at the TU Wien. On the other hand, a comparison with other student theses avoids violations of my personal copyright.

Vienna, 26.03.2023

Sarah Wimmer

Non-disclosure notice:

I would like to point out that the master thesis contains confidential information and internal company data. Therefore, publication or disclosure of contents to third parties is not permitted without the prior consent of the Institute of Process Engineering, Environmental Engineering and Technical Biosciences.

Abstract

Energy is a demanding factor in almost all economic sectors, but only a small amount is provided by renewable sources. The amount must be drastically increased in terms of climate protection. However, renewable energy has some deficits in continuous energy supply, consequently efficient and loss-free energy storage is inevitably necessary. Thermal energy storage bears great potential due to the availability of waste heat from industrial processes. Especially, thermochemical energy storage offers the possibility for efficient, long-term energy storage.

The majority of waste heat is produced in the lower temperature range, thus heat below 200 °C is the focus of this work. Apart from this, a high reaction enthalpy and corresponding high energy storage density are required. Moreover, high cycle stability and the absence of side reactions or thermal decomposition ensure long usage periods. Fast reaction kinetics enable an efficient storage process and high energy output. Of course, low safety risks as well as economic feasibility and availability are additional crucial factors. In order to fulfill these requirements and to achieve efficient and loss-free energy storage, suitable material systems need to be investigated. The aim of this thesis was a systematic screening for reversible gas-solid reaction systems suitable for thermochemical energy storage applications in a suspension reactor.

Several materials were selected based on literature research and subsequently experimentally tested. The storage process was evaluated regarding conversion and dehydration temperature during the charging reaction as well as the temperature increase and corresponding energy output during the discharging reaction. Moreover, side effects like agglomeration, phase change, and foaming were investigated. Several materials showed promising results, but further research is necessary for everyday use.

Kurzfassung

Energie ist in fast allen Wirtschaftsbereichen eine notwendige Komponente, die jedoch nur in geringem Umfang aus erneuerbaren Quellen bereitgestellt wird. Dies muss im Sinne des Klimaschutzes drastisch erhöht werden. Erneuerbare Energien weisen einige Defizite in der kontinuierlichen Energieversorgung auf, folglich ist eine effiziente und verlustfreie Energiespeicherung notwendig. Thermische Energiespeicherung birgt aufgrund der Verfügbarkeit von Abwärme aus industriellen Prozessen ein großes Potenzial. Insbesondere die thermochemische Energiespeicherung bietet die Möglichkeit für eine effiziente und langfristige Speicherung von Energie.

Ein Großteil der Abwärme entsteht im unteren Temperaturbereich und daher steht Wärme unter 200 °C im Fokus dieser Arbeit. Abgesehen davon ist eine hohe Reaktionsenthalpie und entsprechend hohe Energiespeicherdichte erforderlich. Lange Verwendungsperioden werden durch eine hohe Zyklenstabilität und die Abwesenheit von Nebenreaktionen bzw. thermischer Zersetzung sichergestellt. Schnelle Reaktionskinetik ist für einen effizienten Speicherprozess und eine hohe Energieausbeute notwendig. Natürlich sind geringe Sicherheitsrisiken sowie Wirtschaftlichkeit und Verfügbarkeit weitere entscheidende Faktoren. Um diese Anforderungen zu erfüllen und eine effiziente und verlustfreie Energiespeicherung zu erreichen, müssen geeignete Materialsysteme untersucht werden. Das Ziel dieser Arbeit war die Durchführung eines systematischen Screenings nach reversiblen Gas-Feststoff-Reaktionssystemen, die für thermochemische Energiespeicheranwendungen in einem Suspensionsreaktor geeignet sind.

Anhand einer Literaturrecherche wurden mehrere Materialien ausgewählt und anschließend experimentell getestet. Der Speicherprozess wurde hinsichtlich des Umsatzes und der Dehydratisierungstemperatur während der Ladereaktion sowie der Temperaturerhöhung und entsprechender Energieabgabe während der Entladereaktion bewertet. Außerdem wurden Nebeneffekte wie Agglomeration, Phasenumwandlung und Schaumbildung untersucht. Mehrere Materialien zeigten vielversprechende Ergebnisse, aber für den täglichen Gebrauch sind weitere Forschungen notwendig.

Danksagung

An dieser Stelle möchte ich mich aufrichtig bei all jenen Personen bedanken, die mich im Zuge dieser Arbeit und während meines Studiums unterstützt und begleitet haben.

Zuerst möchte ich mich daher bei meinem Betreuer Professor Franz Winter, der mir diese Diplomarbeit ermöglicht hat, bedanken. Ebenso möchte ich mich bei meiner Betreuerin Lena Schmieder bedanken. Ihre Vorschläge und Ideen während des Projekts waren stets hilfreich und die Grundlage vieler Erkenntnisse.

Als Nächstes möchte ich mich bei meinen Arbeitskollegen bedanken. In der Arbeitsgruppe herrschten immer eine großartige Stimmung und ein angenehmes Arbeitsklima. Ihre Erfahrungen und Ratschläge waren eine unglaubliche Unterstützung bei vielen Herausforderungen.

Ebenfalls möchte ich mich bei allen meinen Freunden und Studienkollegen bedanken, die die Studienzeit zu einem spannenden und unglaublichen Erlebnis gemacht haben und für die notwendige Ablenkung zwischen bzw. nach harten Vorlesungs- und Lerntagen gesorgt haben.

Zum Schluss möchte ich mich noch bei meiner Familie bedanken, die mich während meiner Studienzeit immer unterstützt hat. Ohne sie wäre mein Studium so nicht möglich gewesen.

Acknowledgements

The results presented in this thesis are part of the project "**RESTORE - Renewable Energy based seasonal Storage Technology in Order to Raise Environmental sustainability of DHC**" funded by European Union's Horizon 2020 research and innovation program under grant agreement No 101036766.

TU WIEN
Institute of Energy Systems and Thermodynamics
Getreidemarkt 9/E302
A-1060 Wien

TU WIEN
Institute of Chemical, Environmental and Bioscience Engineering
Getreidemarkt 9/E166
A-1060 Wien

Contents

1 Introduction

1.1 Motivation

Energy is a key driver for mankind and its economic activities. Demand for energy was increasing steadily throughout history and the world's energy consumption is predicted to increase even further by nearly 50% between 2018 and 2050 [61]. The main reasons are the growth in world population as well as economic development. Moreover, energy is a dominating factor in political and business deals leading to possible tensions as recent events in history show. In figure 1.1 the increase in the total amount of energy consumption around the world and the respective share of each primary energy source since 1800 are illustrated.

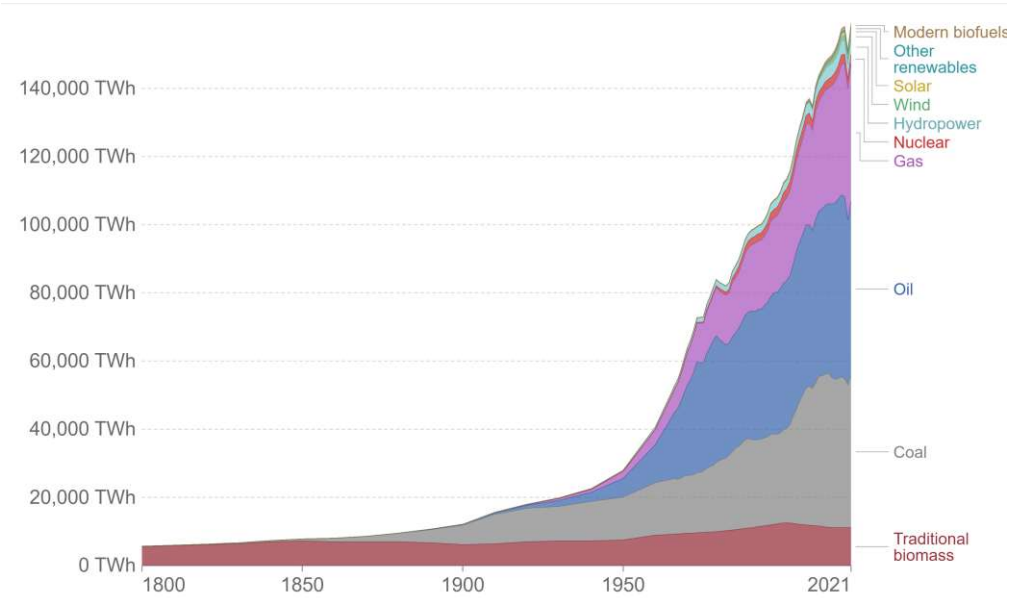

Figure 1.1: Global direct energy consumption and respective share of each primary energy source from 1800 until today [15]

Consumed energy is harvested from various primary energy sources which can be categorized into renewable and non-renewable sources. The quantity of renewable energy was 28% in 2022, although this needs to be drastically increased in terms of climate protection and the accompanying reduction in CO_2 emission [20]. However, renewable energy sources such as solar or hydropower are problematic with temporal fluctuation in availability [25]. Moreover, energy consumption varies over time and thus amplifies the challenges of constant energy supply. In figure 1.2 the time dependence of power generation and consumption in Germany for 2022 are shown.

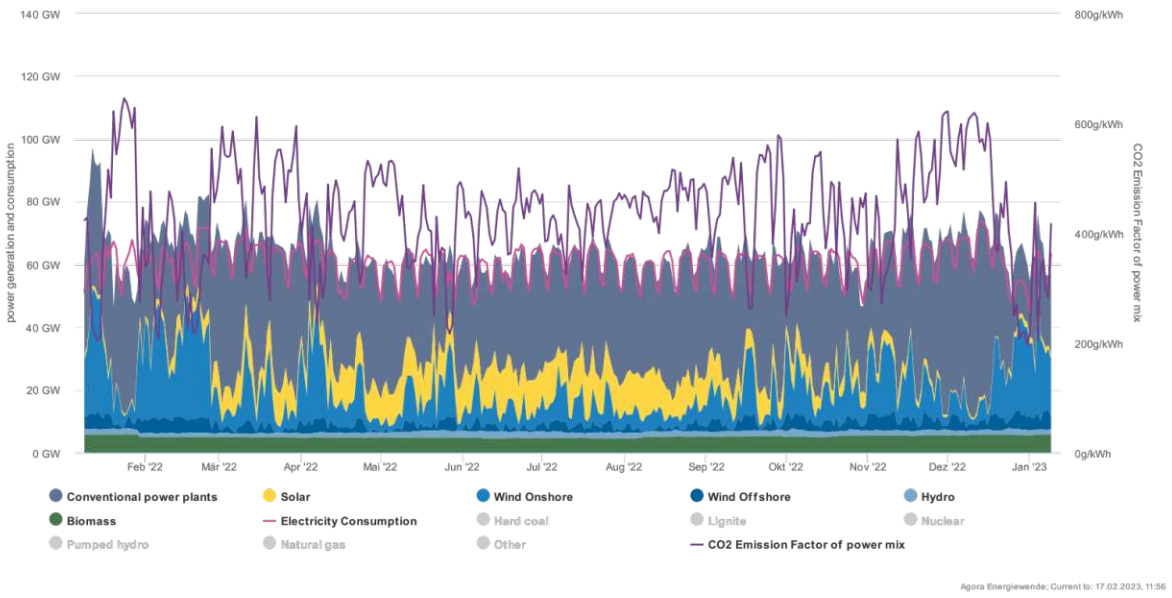

Figure 1.2: Variations in power generation and consumption in Germany for 2022 [1]

A possible solution to overcome deficits of renewable energy is efficient and loss-free energy storage. Particularly thermal energy storage bears great potential due to the availability of waste heat from industrial processes. It is predicted that by 2030 about 50% of the global energy consumption will end up as waste heat with a theoretical recovery potential of 6–12% [13]. In figure 1.3 the distribution of energy consumption and according temperature in the European Union are shown for different industrial sectors.

The majority of waste heat is produced in the lower temperature range (60-120°C) as well as the upper-temperature range over 1400°C [23]. The lower temperature range offers great potential for thermal energy storage, and thus will be the focus of this work. Thermal storage can be achieved in different ways such as sensible, latent, or thermochemical [5]. Of course, each system has advantages and disadvantages in different application areas. Nevertheless, for long-term storage, thermochemical energy storage (TCES) seems the most promising, as a high energy density (specific thermal storage capacity) and negligible heat loss can be achieved [44]. TCES bears a lot of potential, but still, a lot of research is necessary for commercial use. Especially, suitable material systems need to be investigated in order to achieve efficient and loss-free energy storage.

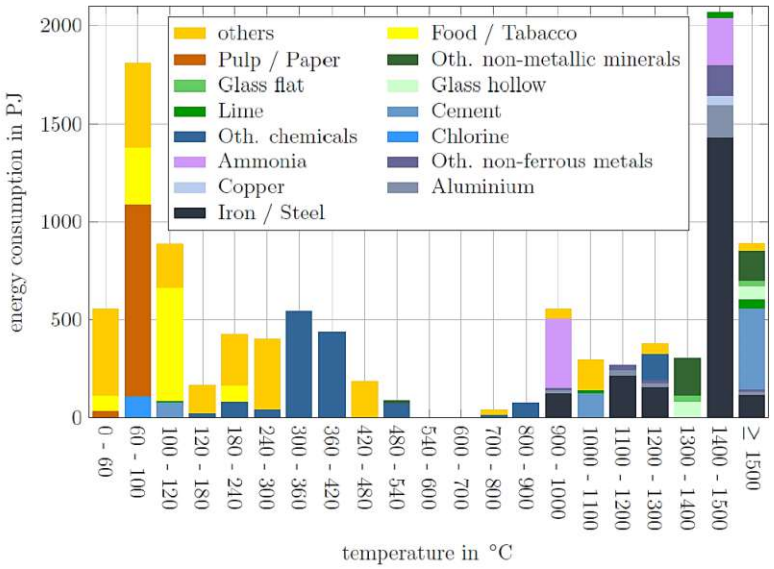

Figure 1.3: Energy consumption and temperature of industrial sectors in the EU-27 [23]

1.2 Aim

Energy storage is of great importance to overcome several energy production and consumption challenges we face nowadays. Especially, TCES bears great potential for efficient, long-term energy storage [44]. The aim of this thesis is a systematic screening for reversible gas-solid reaction systems suitable for thermochemical energy storage. The main requirements for innovative material systems are a high storage density, high specific reaction enthalpy, and sufficient cyclability as well as suitability for suspension reactor conditions. The reaction conditions in a suspension reactor are limited according to the available temperature range for dehydration reaction and due to the occurrence of process challenges such as foaming and agglomeration. Various material systems are tested for their energy storage potential and evaluated according to their overall properties.

1.3 Methodology of the thesis

New reaction systems are carefully selected according to their properties by previous literature research and experimentally tested in a reactor system to get information regarding thermodynamic data as well as conversion rate, and cyclability. The screening procedure started by identifying salt hydrates from chemical databases and literature. In the first step a theoretical analysis was accomplished, by evaluating the availability, toxicity, as well as chemical and thermodynamic properties. Subsequently, thermal stability and theoretical temperature of dehydration were investigated by evaluating thermogravimetric analysis (TGA) measurements. Moreover, possible side reactions and reversibility of the process were studied. Finally, energy density, specific reaction enthalpy, and to a minor part also costs were investigated. Material systems that did not meet all requirements were excluded from experimental testing.

2 Theoretical background and state of the art

2.1 Fundamentals of thermal energy storage

Nowadays, a wide variety of energy storage techniques are known, such as electrical, mechanical, chemical, and thermal energy storage, depending on which type of energy is utilised. Thermal energy storage is generally based on storing heat, nevertheless, can be divided into three categories depending on the respective working principle, as stated in figure 2.1.

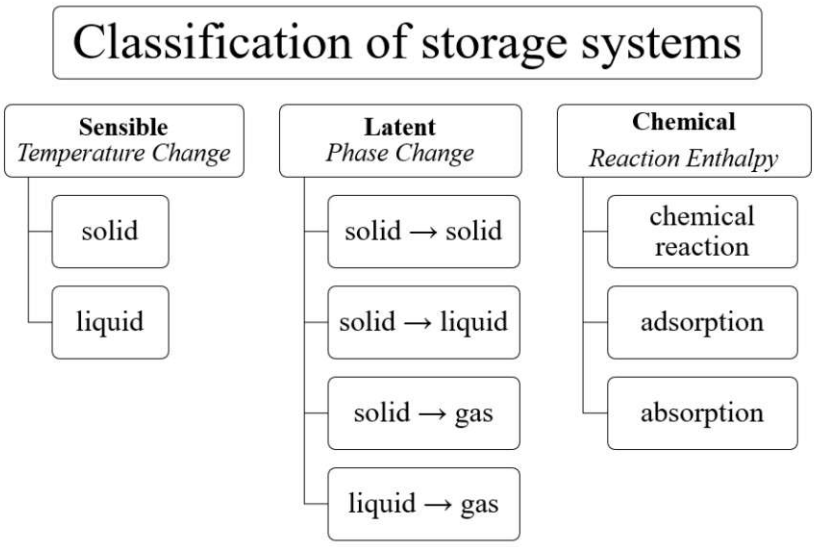

Figure 2.1: Classification of thermal energy storage systems

Thermal energy storage is categorized into sensible, latent, and chemical energy storage. The working principle of sensible heat storage is simple but effective. Heat is stored, by heating the storage medium, such as water, and subsequently insulating the material efficiently until release. Temperature difference, heat capacity, and mass of the storage medium determine the amount of stored energy. Latent heat storage is based on a change in the state of aggregation through the supply of heat to the system. Commonly, the solid-liquid phase change is used, therefore heat is stored by melting the material and subsequently released when the material solidifies again [5]. The phase change enthalpy and mass of the storage medium as well as the temperature difference and heat capacity determine the amount of stored energy. Thermochemical energy storage utilizes the reaction enthalpy of a reversible reaction for heat storage. Thermochemical energy storage

is classified into chemical reactions and sorption processes. In general, heat is applied to induce the endothermic reaction or desorption process, leading to storable reaction products. Thus, heat is stored as reaction enthalpy and can be retrieved during the reverse reaction or ad-/absorption.

2.2 Principle of thermochemical energy storage

The principle of thermochemical energy storage is based on reversible chemical reactions or reversible sorption processes leading to a change in the composition of the storage material [9]. Thus, energy is stored as reaction enthalpy ΔH_r, as given in the general reaction equation 2.1.

$$\nu_A A_{(s)} + \Delta H_r \rightleftharpoons \nu_B B_{(s)} + \nu_C C_{(g/l)} \tag{2.1}$$

During the charging reaction, material A decomposes through energy input, leading to the formation of a storable solid component B (charged material) and a gaseous or liquid component C. The discharging reaction is based on the reverse reaction of components B and C generating component A and thereby releasing stored energy. An unintended reverse reaction is prevented by separate storage of components B and C. It has to be mentioned that not all systems follow this general reaction equation. The general working principle utilized for this work is visualized in the flowchart 2.2. Both processes, discharging and charging are shown.

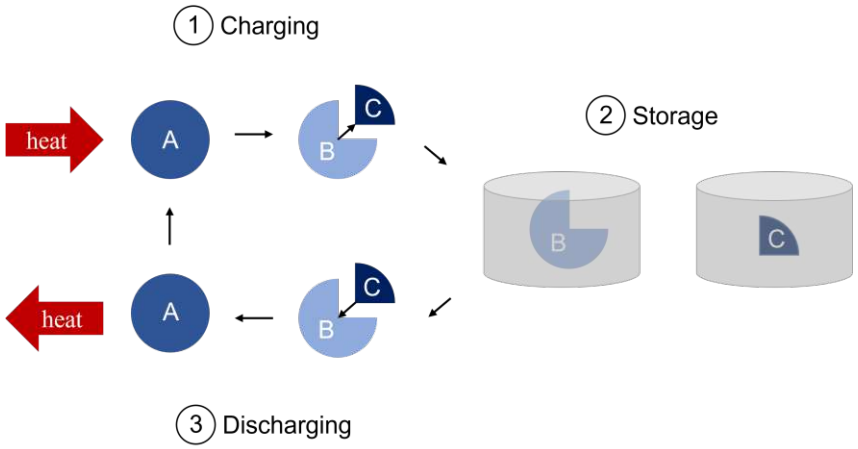

Figure 2.2: Flowchart of the general working principle of TCES utilized for this work

2.3 State of the Art - Material systems

The utilized storage material strongly affects the performance of energy storage systems, thus the material selection is a crucial part of the development of energy storage applications [44]. Recently, there has been a high research interest in the discovery of innovative materials for both thermochemical storage in low and high temperature applications as well as sorption processes. Nevertheless, several difficulties to meet the expectations occurred. General requirements which should be fulfilled by a TCES material are:

- high reaction enthalpy
- high energy storage density
- no thermal loss during storage
- high cycle stability
- high conversion in the required temperature range
- no side reactions or thermal decomposition
- fast reaction kinetic for high thermal energy output
- low safety risks
- economic feasibility and availability

In more detail, a high reaction enthalpy is required as it determines the energy output of the storage system. The theoretical reaction enthalpy Δh_R° can be calculated according (2.2) using the standard formation enthalpy h_f° of all reactants considering the stoichiometric coefficients ν.

$$\Delta h_R^\circ = \sum_{i\ products} \nu_i h_{f,i}^\circ - \sum_{j\ educts} \nu_j h_{f,j}^\circ \tag{2.2}$$

The sum of all standard formation enthalpies $h_{f,i}^\circ$ of the products subtracted by the sum of all standard formation enthalpies $h_{f,i}^\circ$ of the educts results in the reaction enthalpy Δh_R°. Following, the theoretical energy storage density Δh_m° as well as Δh_V° can be calculated in (2.3) and (2.4) .

$$\Delta h_m^\circ = \frac{\Delta h_R^\circ}{M} \tag{2.3}$$

$$\Delta h_V^\circ = \Delta h_m^\circ \cdot \rho \tag{2.4}$$

The theoretical reaction enthalpy Δh_R° is divided by the molar mass M of the educt (component A) resulting in Δh_m°. Subsequently Δh_V° is calculated with the density ρ of the educt (component A). Depending on the state of aggregation of the added water (liquid or gaseous) to the system (component C) two different energy storage densities can be calculated.

Low thermal loss during storage is necessary to achieve highly efficient storage applications. Moreover, a high conversion in the required temperature range and the absence of side reactions as well as thermal decomposition are important to achieve high efficiency. Fast reaction kinetics are important for high energy output, but also for efficient charging. Additionally, high cycle stability is required to ensure long usage periods. Low safety risks, economic feasibility and availability are self-explanatory.

However, the requirements for storage materials in this work are more specific and characterized by:

- high experimental reaction enthalpy
- high experimental energy storage density
- cycle stability for several runs
- high conversion below 200 °C
- no agglomeration or phase change phenomena
- fast reaction kinetic for the discharging reaction
- no reaction with the suspension medium
- economic feasibility and availability
- low environmental impact
- low foaming

2.4 Material systems

Various promising material systems for TCES applications have been carefully selected and experimentally tested. Important theoretical values have been collected and clearly stated in table 2.1.

Table 2.1: Overview of the theoretical material data of all examined systems based on [19, 46, 64]

Substance	**CAS no.**	**M**	**Density ρ**	**Δh_V° (H_2O)**	**Δh_m° ($H_2O_{(l)}$)**	**Heat capacity c_P**	**Costs**
		g/mol	*kg/m³*	*MJ/m³*	*kJ/kg*	*kJ/(kg K)*	
$MgSO_4 \cdot 7\,H_2O$	10034-99-8	246.5	1680	2236	260	1.54	€
$ZnSO_4 \cdot 7\,H_2O$	7446-20-0	287.5	1970	2220	215	1.33	€
$FeSO_4 \cdot 7\,H_2O$	7782-63-0	278.0	1890	2200	210	1.42	€€
$Al_2(SO_4)_3 \cdot 18\,H_2O$	7784-31-8	342.2	1610	2600	80	1.48	€€
$K_2Zn(SO_4)_2 \cdot 6\,H_2O$	7790-65-0	443.8	2242	1785	191	0.10	-
$K_2Mg(SO_4)_2 \cdot 6\,H_2O$	-	402.7	2050	1700	190	0.11	-
$K_2Cu(SO_4)_2 \cdot 6\,H_2O$	-	442.0	2232	1850	225	0.10	-
$SrBr_2 \cdot 6\,H_2O$	7789-53-9	355.5	2386	1941	195	0.97	€€€
Zeolite 4A	70955-01-0	202.1	600	720	-	0.94	€€
$MgCl_2 \cdot 6\,H_2O$	7791-18-6	203.3	1569	1945	374	1.55	€
$SrCl_2 \cdot 6\,H_2O$	10025-70-4	266.6	1930	2030	220	0.30	€€€
$K_2C_2O_4 \cdot H_2O$	6487-48-5	184.2	2140	650	70	0.25	€€
$CaSO_4 \cdot 2\,H_2O$	10101-41-4	172.2	2320	1366	78	1.08	€
$MgBr_2 \cdot 6\,H_2O$	13446-53-2	292.2	2000	2976	584	0.16	€€€
$MnSO_4 \cdot 4\,H_2O$	15244-36-7	223.1	2110	2064	108	0.24	€€€

2.4.1 Magnesium sulphate

Magnesium sulphate ($MgSO_4$) can form various hydrates $MgSO_4 \cdot n\,H_2O$ with n between 1 and 11. Magnesium sulphate heptahydrate ($MgSO_4 \cdot 7\,H_2O$) is the most frequently occurring hydrate and is commonly known as Epsom salt. Theoretical analyses indicated $MgSO_4 \cdot 7\,H_2O$ as a promising thermochemical storage material based on the reversible hydration reaction in (2.5) [49, 63].

$$MgSO_4 + 7\,H_2O \rightleftharpoons MgSO_4 \cdot 7\,H_2O + \Delta H_r \tag{2.5}$$

Six molecules of water are octahedrally bonded to the magnesium ion, the seventh is attached to the sulphate ion via hydrogen bonding [52]. Several dehydration mechanisms have been reported [49, 52, 63]. The general mechanism indicates that the first six molecules of water are lost in one step at around 150 °C written in (2.6) and in a second step at 200 °C the anhydrous salt is formed given in (2.7) [52].

$$MgSO_4 \cdot 7\,H_2O \rightleftharpoons MgSO_4 \cdot H_2O + 6\,H_2O \tag{2.6}$$
$$MgSO_4 \cdot H_2O \rightleftharpoons MgSO_4 + H_2O \tag{2.7}$$

The reaction enthalpy for the reaction of $MgSO_4 \cdot 7\,H_2O$ to $MgSO_4 \cdot H_2O$ is 328 kJ/mol with gaseous water and 64 kJ/mol with liquid water [46]. Following, the theoretically available energy density with gaseous water is 2236 MJ/m^3 and 260 kJ/kg with liquid water. The heat capacity of $MgSO_4 \cdot 7\,H_2O$ is 1.54 kJ/(kg K) at 25 °C [16].

However, thermogravimetric analysis (TGA) and differential scanning calorimetry (DSC) measurements with a heating rate of 1 °C/min showed that heating $MgSO_4 \cdot 7\,H_2O$ leads to a different stepwise dehydration depending on temperature. First, the heptahydrate reacts to the hexahydrate with the elimination of one water molecule at around 25-55 °C, as stated in (2.8) [63]. Further heating leads to the conversion of the hexahydrate to $MgSO_4 \cdot 0.1\,H_2O$ at around 150 °C, given in (2.9) [49, 63]. The conversion to the anhydrous salt, shown in (2.10) requires temperatures over 275 °C, thus this reaction is not considered for suspension reactor conditions [63].

$$MgSO_4 \cdot 7\,H_2O \rightleftharpoons MgSO_4 \cdot 6\,H_2O + H_2O \tag{2.8}$$
$$MgSO_4 \cdot 6\,H_2O \rightleftharpoons MgSO_4 \cdot 0.1\,H_2O + 5.9\,H_2O \tag{2.9}$$
$$MgSO_4 \cdot 0.1\,H_2O \rightleftharpoons MgSO_4 + 0.1\,H_2O \tag{2.10}$$

Apart from the good thermodynamic properties, the main advantages of $MgSO_4 \cdot 7\,H_2O$ are the low costs of only 60 €/kg (ReagentPlus®, ≥ 99.0%), high availability of more than 100 kt/a in the European Economic Area, and no safety risks [11, 28].

2.4.2 Zinc sulphate

Zinc sulphate heptahydrate ($ZnSO_4 \cdot 7\,H_2O$) is a promising thermochemical energy storage material due to attractive properties such as high theoretical energy storage density, long storage stability and reversible hydration reaction, as well as low costs together with great availability [49, 50]. The energy storage is based on the hydration reaction in (2.11).

$$ZnSO_4 + 7\,H_2O \rightleftharpoons ZnSO_4 \cdot 7\,H_2O + \Delta H_r \tag{2.11}$$

$ZnSO_4$ itself exists in different hydrate levels, depending on temperature and composition. These various hydrates play a major role in the dehydration reaction of $ZnSO_4 \cdot 7\,H_2O$ and thus in the energy storage charging process [50]. Theoretically, the heptahydrate reacts to the hexahydrate with the elimination of one water molecule at around 39 °C, as stated in (2.12). Further dehydration leads to the conversion of the hexahydrate to the monohydrate at 70 °C, stated in (2.13). The conversion to the anhydrate, shown in (2.14) requires temperatures over 238 °C , thus this reaction is not considered for suspension reactor conditions [4].

$$ZnSO_4 \cdot 7\,H_2O \rightleftharpoons ZnSO_4 \cdot 6\,H_2O + H_2O \tag{2.12}$$
$$ZnSO_4 \cdot 6\,H_2O \rightleftharpoons ZnSO_4 \cdot H_2O + 5\,H_2O \tag{2.13}$$
$$ZnSO_4 \cdot H_2O \rightleftharpoons ZnSO_4 + H_2O \tag{2.14}$$

Surprisingly, TGA and DSC measurements indicate different stable and unstable stages between 20-150 °C [50]. Two stable mass loss stages, first from heptahydrate to pentahydrate and second from pentahydrate to monohydrate are observed [49]. Moreover, the first dehydration step in the range of 30 °C to 57 °C contains two additional transition stages at 33 °C ($7 \rightarrow 6\beta$) and 38 °C ($6\beta \rightarrow 6\alpha$). In the second dehydration step, four moles of water are lost between 60 °C to 110 °C [50].

However, the resulting reaction enthalpy for the conversion of heptahydrate to monohydrate is 326 kJ/mol with gaseous water and 62 kJ/mol with liquid water [46]. The according theoretical energy density with gaseous water is 2220 MJ/m^3 and 215 kJ/kg with liquid water. The heat capacity is 1.33 kJ/(kg K) at 25 °C [19]. Apart from the good thermodynamic properties, safety risks of zinc sulphate heptahydrate need to be considered, as it is very toxic to aquatic life, causes serious eye-damage, is harmful if swallowed,

causes skin irritation, and may cause respiratory irritation [11]. The production of zinc sulphate is based on dissolving zinc or zinc oxide in sulfuric acid [4]. The resulting product zinc sulphate can be hydrated in order to obtain zinc sulphate heptahydrate. As already mentioned above, the main advantages of zinc sulphate are the low costs of only 70 €/kg (ReagentPlus®, ≥ 99.0%) and the high availability as it is manufactured or imported to the European Economic Area with more than 10 kt/a [11, 39].

2.4.3 Iron sulphate

Iron sulphate heptahydrate shows promising properties similar to $ZnSO_4 \cdot 7\,H_2O$, such as high storage density, low dehydration temperature, and low costs. Nevertheless, $FeSO_4 \cdot 7\,H_2O$ is relatively unknown as TCES material [49]. The energy storage process is based on the reaction given in (2.15).

$$FeSO_4 + 7\,H_2O \rightleftharpoons FeSO_4 \cdot 7\,H_2O + \Delta H_r \tag{2.15}$$

Iron sulphate itself exists, like magnesium and zinc sulphate, in different hydrate levels, depending on temperature and composition. Increasing the temperature leads to a stepwise dehydration of $FeSO_4 \cdot 7\,H_2O$. First, the heptahydrate reacts to the tetrahydrate with the elimination of three water molecules at around 32-57 °C, as stated in (2.16). The next step involves the conversion of tetrahydrate to monohydrate at around 80-110 °C, shown in (2.17) [49]. The conversion to the anhydrate, stated in (2.18) requires temperatures of 200-400 °C, thus this reaction is not considered for suspension reactor conditions [22].

$$FeSO_4 \cdot 7\,H_2O \rightleftharpoons FeSO_4 \cdot 4\,H_2O + 3\,H_2O \tag{2.16}$$
$$FeSO_4 \cdot 4\,H_2O \rightleftharpoons FeSO_4 \cdot H_2O + 3\,H_2O \tag{2.17}$$
$$FeSO_4 \cdot H_2O \rightleftharpoons FeSO_4 + H_2O \tag{2.18}$$

The reaction enthalpy for the reaction from iron sulphate heptahydrate to monohydrate is 321 kJ/mol with gaseous water and 58 kJ/mol with liquid water [46]. The according theoretical energy density with gaseous water is 2200 MJ/m^3 and 210 kJ/kg with liquid water. The heat capacity is 1.42 kJ/(kg K) at 25 °C [19]. Apart from the promising thermodynamic properties, the main advantages of this TCES medium are the low costs in technical grade (85-90% purity) as well as the high availability of up to 10 Mt/a manufacturing and import to the European Economic Area [11]. For comparison, analytical grade iron sulphate heptahydrate costs 200 €/kg (ReagentPlus®, ≥ 99.0%) [32]. Iron sulphate is produced in large quantities as a by-product during steel finishing and titanium dioxide production [66]. It needs to be considered that iron sulphate heptahydrate causes serious eye irritation, is harmful if swallowed, and causes skin irritation [11].

2.4.4 Aluminium sulphate

Aluminium sulphate octadecahydrate ($Al_2(SO_4)_3 \cdot 18\,H_2O$) is a suitable TCES material, as theoretically dehydration reaction is reversible, no side reactions occur, and the theoretical storage density is high [44]. Moreover, the costs are low together with relatively high availability. The energy storage is based on the hydration reaction of $Al_2(SO_4)_3 \cdot 18\,H_2O$, given in (2.19).

$$Al_2(SO_4)_3 + 18\,H_2O \rightleftharpoons Al_2(SO_4)_3 \cdot 18\,H_2O + \Delta H_r \tag{2.19}$$

However, the identification of dehydration stages and accompanying water loss is crucial for the use of $Al_2(SO_4)_3 \cdot 18\,H_2O$ as TCES material. TGA and DSC measurements indicate various stable and unstable stages between 50-700 °C [7]. The first stage consists of the dehydration reaction of the octadecahydrate to the hexadecahydrate with the elimination of two water molecules at around 52-81 °C, as shown in (2.20) [7].

$$Al_2(SO_4)_3 \cdot 18\,H_2O \rightleftharpoons Al_2(SO_4)_3 \cdot 16\,H_2O + 2\,H_2O \tag{2.20}$$

The product $Al_2(SO_4)_3 \cdot 16\,H_2O$ forms at reaction state and is unstable at ambient conditions [7]. In the second stage, the conversion from the hexadecahydrate to the hexahydrate at around 81-164 °C takes place, as given in (2.21).

$$Al_2(SO_4)_3 \cdot 16\,H_2O \rightleftharpoons Al_2(SO_4)_3 \cdot 6\,H_2O + 10\,H_2O \tag{2.21}$$

$Al_2(SO_4)_3 \cdot 6\,H_2O$ is a stable hydrate salt. Further dehydration during the third stage leads to anhydrous $Al_2(SO_4)_3$, stated in (2.25), though is divided into three substages. The first substage consists of a gradual loss of three moles of water at 164-307 °C and thus the formation of $Al_2(SO_4)_3 \cdot 3\,H_2O$ given in (2.22). During the second and third substage, further dehydration reaction takes place ending with the arise of anhydrous $Al_2(SO_4)_3$ at around 700 °C, as written in (2.23) and (2.24) [7]. Since the required temperature for the third stage exceeds the requirements of the suspension reactor system, this stage is not considered for thermochemical energy storage.

$$Al_2(SO_4)_3 \cdot 6\,H_2O \rightleftharpoons Al_2(SO_4)_3 \cdot 3\,H_2O + 3\,H_2O \quad (2.22)$$
$$2\,Al_2(SO_4)_3 \cdot 6\,H_2O \rightleftharpoons Al_4(SO_4)_6 \cdot 3\,H_2O + 3\,H_2O \quad (2.23)$$
$$Al_4(SO_4)_6 \cdot 3\,H_2O \rightleftharpoons 2Al_2(SO_4)_3 + 3\,H_2O \quad (2.24)$$
$$Al_2(SO_4)_3 \cdot 6\,H_2O \rightleftharpoons Al_2(SO_4)_3 + 6\,H_2O \quad (2.25)$$

The reaction enthalpy for the reaction from $Al_2(SO_4)_3 \cdot 18\,H_2O$ to $Al_2(SO_4)_3 \cdot 6\,H_2O$ is 555 kJ/mol with gaseous water and only 27 kJ/mol with liquid water [64]. Thus the available theoretical energy density with gaseous water is 2600 MJ/m^3 but only 80 kJ/kg with liquid water. The heat capacity is 1,48 kJ/(kg K) at 25°C [19]. The costs of $Al_2(SO_4)_3 \cdot 18\,H_2O$ are 115 €/kg ($\geq$ 97%) [29]. Moreover, the anhydrous salt has a relatively high availability of more than 100 kt/a in the European Economic Area [11]. Aluminium sulphate hydrates are produced by dissolving pure aluminium oxide or aluminium hydroxide in concentrated sulfuric acid by the Giulini process [17]. Apart from the appealing thermodynamic and economic properties, it needs to be mentioned that this salt causes serious eye damage and may be corrosive to metals [11].

2.4.5 Tutton's salts

Tutton's salts are a class of isomorphous monoclinic crystals with the general formula $M^I_2M^{II}(SO_4)_2(H_2O)_6$. The crystal unit cell comprises two octahedral hexahydrate complexes $[M^{II}(H_2O)_6]^{2+}$, with M^{II} being a divalent cation (Co, Zn, Fe, ion of the 3d group), and M^I being a monovalent cation (Na, K, Rb, Cs) [24]. Recently, Tutton's salts are of high interest due to promising properties for several applications, for example as strong energy absorbers in solar collectors [56]. Unfortunately, Tutton's salts are not commercially available resulting in economic challenges for large-scale applications. Nevertheless, Tutton's salts are worth a look as preliminary tests for TCES showed promising results.

$K_2Zn(SO_4)_2 \cdot 6\,H_2O$

Theoretical analysis indicated $K_2Zn(SO_4)_2 \cdot 6\,H_2O$ as a promising thermochemical storage material, due to the high theoretical energy density. The energy storage process is based on the reversible hydration reaction in (2.26).

$$K_2Zn(SO_4)_2 + 6\,H_2O \rightleftharpoons K_2Zn(SO_4)_2 \cdot 6\,H_2O + \Delta H_r \quad (2.26)$$

The reaction enthalpy for this reaction is 353 kJ/mol with gaseous water and 85 kJ/mol with liquid water [64]. Resulting, $K_2Zn(SO_4)_2 \cdot 6\,H_2O$ has a theoretical energy density with gaseous water of 1785 MJ/m^3 and an energy density with liquid water of 191 kJ/kg.

The heat capacity is 0.10 kJ/(kg K) at 25°C [19]. On the one hand, TGA measurements indicate that six water molecules left the system in one step at around 80-110 °C. On the other hand, DSC measurements indicate that water is lost in two stages with the occurrence of intermediates [42]. Since the anhydrous salt is obtained in any case, the influence of possible intermediates on the energy storage process is considered as low. Thus, this topic will not be further investigated in the course of this work.

This Tutton salt is obtained by dissolving equimolar amounts of potassium sulphate and zinc sulphate heptahydrate and subsequent crystallization by evaporation. Since this salt is a 1:1 combination of potassium sulphate and zinc sulphate heptahydrate the costs can be estimated from the educt's costs, resulting in 75 €/kg [36, 39]. Additional production costs are not taken into account. Information regarding safety risks is not available.

$K_2Mg(SO_4)_2 \cdot 6\,H_2O$

Similarly, $K_2Mg(SO_4)_2 \cdot 6\,H_2O$ shows promising properties such as high energy storage density. Moreover, it might be a good alternative to magnesium sulphate heptahydrate which causes difficulties during the storage process. The energy storage is based on the reaction written in (2.27).

$$K_2Mg(SO_4)_2 + 6\,H_2O \rightleftharpoons K_2Mg(SO_4)_2 \cdot 6\,H_2O + \Delta H_r \tag{2.27}$$

The reaction enthalpy for this reaction is 333 kJ/mol with gaseous water and 75 kJ/mol with liquid water [64]. The theoretical energy density with gaseous water is 1700 MJ/m^3 and 190 kJ/kg with liquid water for $K_2Mg(SO_4)_2 \cdot 6\,H_2O$. The heat capacity at 25 °C is 0.11 kJ/(kg K) [19]. Various dehydration pathways with different intermediates have been reported [42]. Several TGA and DSC measurements suggest a reaction pathway including the formation of four intermediate products [56]. In the first stage, $K_2Mg(SO_4)_2 \cdot 6\,H_2O$ is dehydrated to $K_2Mg(SO_4)_2 \cdot 5\,H_2O$ at 25-70 °C as written in (2.28). Following, the intermediate product $K_2Mg(SO_4)_2 \cdot 5\,H_2O$ is dehydrated to $K_2Mg(SO_4)_2 \cdot 1.5\,H_2O$ at 70-128 °C, shown in (2.29). The third step is the dehydration of $K_2Mg(SO_4)_2 \cdot 1.5\,H_2O$ to the monohydrate $K_2Mg(SO_4)_2 \cdot H_2O$ at 128-145 °C, written in (2.30). The last dehydration step is at 145-180 °C leading to the formation of the anhydrous salt in (2.31) [56].

$$K_2Mg(SO_4)_2 \cdot 6\,H_2O \rightleftharpoons K_2Mg(SO_4)_2 \cdot 5\,H_2O + H_2O \tag{2.28}$$
$$K_2Mg(SO_4)_2 \cdot 5\,H_2O \rightleftharpoons K_2Mg(SO_4)_2 \cdot 1.5\,H_2O + 3.5\,H_2O \tag{2.29}$$
$$K_2Mg(SO_4)_2 \cdot 1.5\,H_2O \rightleftharpoons K_2Mg(SO_4)_2 \cdot H_2O + 0.5\,H_2O \tag{2.30}$$
$$K_2Mg(SO_4)_2 \cdot H_2O \rightleftharpoons K_2Mg(SO_4)_2 + H_2O \tag{2.31}$$

$K_2Mg(SO_4)_2 \cdot 6\,H_2O$ is obtained through the dissolution of equimolar amounts of potassium sulphate and magnesium sulphate heptahydrate and subsequent evaporation leading to crystallization [56]. Thus, the costs for the product can be estimated based on the educt's costs, resulting in 70 €/kg [28, 36]. Additional production costs are not taken into account. Information regarding safety risks is not available.

$K_2Cu(SO_4)_2 \cdot 6\,H_2O$

$K_2Cu(SO_4)_2 \cdot 6\,H_2O$ might be usable as an efficient TCES material, yet little information is known on energy storage properties and applications. Theoretically, the energy storage process is based on the reaction written in (2.32).

$$K_2Cu(SO_4)_2 + 6\,H_2O \rightleftharpoons K_2Cu(SO_4)_2 \cdot 6\,H_2O + \Delta H_r \tag{2.32}$$

The reaction enthalpy for this reaction is 367 kJ/mol with gaseous water and 99 kJ/mol with liquid water [64]. Consequently, $K_2Cu(SO_4)_2 \cdot 6\,H_2O$ has a theoretical energy density with gaseous water of 1850 MJ/m^3 and 225 kJ/kg with liquid water. The heat capacity is 0.10 kJ/(kg K) at 25 °C [19]. During the dehydration process, two clearly resolved endothermic transitions were observed in TGA and DSC measurements [42]. The first transition from $K_2Cu(SO_4)_2 \cdot 6\,H_2O$ to $K_2Cu(SO_4)_2 \cdot 2\,H_2O$ taking place at 25-81 °C is given in (2.33). The second dehydration from the dihydrate to the anhydrous salt occurs at 81-153 °C in (2.34) [56].

$$K_2Cu(SO_4)_2 \cdot 6\,H_2O \rightleftharpoons K_2Cu(SO_4)_2 \cdot 2\,H_2O + 4\,H_2O \tag{2.33}$$
$$K_2Cu(SO_4)_2 \cdot 2\,H_2O \rightleftharpoons K_2Cu(SO_4)_2 + 2\,H_2O \tag{2.34}$$

Similar to the Tutton salts above, $K_2Cu(SO_4)_2 \cdot 6\,H_2O$ can be produced by dissolving equimolar amounts of potassium sulphate and copper sulphate hexahydrate followed by evaporation for crystallization [56]. The evaporation process must be conducted slowly in order to achieve high yields. Fast evaporation leads to the formation of a green side product $KCu_2(SO_4)_2[(OH)(H_2O)]$ [47]. The costs for this Tutton's salt can again be estimated based on the educt's costs, resulting in about 100 €/kg [36], [31]. Additional production costs are not taken into account. Information regarding safety risks is not available.

2.4.6 Strontium bromide

Strontium bromide is a potentially promising salt for thermochemical energy storage as thermodynamic properties are appealing. Moreover, it offers a high energy storage potential at a charging temperature below 105 °C [44]. The utilisation of $SrBr_2 \cdot 6\,H_2O$ as TCES material is based on the reaction in (2.35).

$$SrBr_2 + 6\,H_2O \rightleftharpoons SrBr_2 \cdot 6\,H_2O + \Delta H_r \tag{2.35}$$

The dehydration process itself takes place in three steps. The first step is the transition from the hexahydrate to $SrBr_2 \cdot 1.8\,H_2O$ at 91°C, as given in (2.36). In the second step,

the monohydrate salt is formed at 144 °C, given in (2.37). In the third stage at 198 °C, the anhydrous salt is formed in (2.38), thus this reaction step is not considered for energy storage applications in low temperature range [2].

$$SrBr_2 \cdot 6\,H_2O \rightleftharpoons SrBr_2 \cdot 1.8\,H_2O + 4.2\,H_2O \tag{2.36}$$

$$SrBr_2 \cdot 1.8\,H_2O \rightleftharpoons SrBr_2 \cdot H_2O + 0.8\,H_2O \tag{2.37}$$

$$SrBr_2 \cdot H_2O \rightleftharpoons SrBr_2 + H_2O \tag{2.38}$$

The dehydration reaction from the hexahydrate to monohydrate has a reaction enthalpy of 289 kJ/mol with gaseous water and 69 kJ/mol with liquid water [46]. Accordingly, the theoretical energy density with gaseous water is 1941 MJ/m^3 and 195 kJ/kg with liquid water. The heat capacity is 0.97 kJ/(kg K) at 25 °C [19]. Even though the anhydrous salt is stable up to 643 °C, the hexahydrate already melts at a temperature of 89 °C [57]. This needs to be considered as various phase change phenomena like agglomeration might occur. Moreover, strontium bromide is very expensive at 350 €/kg (99%) due to its limited production [60]. The production is based on the reaction of strontium carbonate, obtained from the rare mineral celestine or strontianite, with hydrobromic acid and water [14]. However, since strontium bromide is highly expected to be a promising energy storage material at a low temperature level, innovative and economic ways of production are currently investigated [14].

2.4.7 Zeolite 4A

Zeolite and zeolite composite materials as thermochemical energy storage materials are highly investigated at present. These material systems meet the requirements of high energy storage density, attractive adsorption properties as well as efficient heat and mass transfer. The principle of energy storage is based on sorption, more precisely adsorption and desorption are accompanied by a change of energy. The necessary adsorption property is primarily achieved through the microporous structure of the materials [12]. Many conventional zeolites like 4A or 13X show a type I adsorption isotherm, as depicted in figure 2.3 [12]. During the charging process, energy is applied and consequently water desorbed from the microporous structure of the zeolite. During discharging, water gets adsorbed again and heat is released.

Zeolitic systems reach theoretical energy storage densities up to 720 MJ/m^3 [53]. Nevertheless, in order to achieve a high energy storage density, high temperatures of up to 180 °C are required during the charging process [40]. This might be a disadvantage for the usage of zeolites as TCES material in low temperature applications. Zeolites are synthesized from various natural sources such as clay, kaolin, fly ash, coal, natural oxide, bauxite, feldspar, activated carbon, and other silica sources [8]. Commonly, the hydrothermal synthesis method is utilized, which consists of two stages, the initial for-

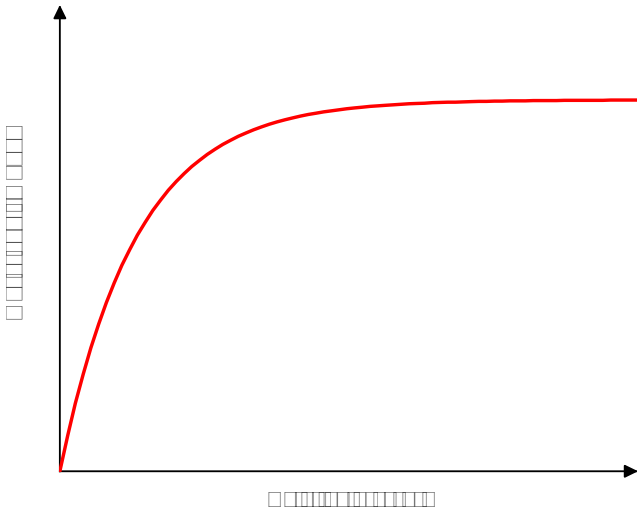

Figure 2.3: Exemplary illustration of a type I adsorption isotherm

mation of hydrated aluminosilicate gel and the subsequent crystallization stage [43, 45]. The price of zeolite 4A is about 120 €/kg (beads, 1.6-2.6 mm) [38]. According to safety regulations, zeolites are harmful in contact with skin, cause serious eye irritation and may cause respiratory irritation [11].

2.4.8 Magnesium chloride

Magnesium chloride hydrates are appealing as TCES salt in low temperature applications. $MgCl_2$ can form several hydrates $MgCl_2 \cdot n\,H_2O$ with $n = 12, 8, 6, 4, 2, 1$. In large-scale production, the hexahydrate is obtained, which is octahedrally coordinated to six water ligands [54]. The TCES process relies on the following reaction in (2.39).

$$MgCl_2 + 6\,H_2O \rightleftharpoons MgCl_2 \cdot 6\,H_2O + \Delta H_r \tag{2.39}$$

The thermal dehydration of the hexahydrate is not straightforward as different intermediate hydrates are formed. First, the hexahydrate loses two water molecules and the tetrahydrate is formed at around 69 °C as given in (2.40). In the second step, the dihydrate is formed at a temperature of 129 °C, shown in (2.41) [18]. Following, the monohydrate occurs at around 167 °C in (2.42) [18]. Anhydrous $MgCl_2$ cannot be obtained directly through thermal dehydration since thermal decomposition with the release of hydrochloric acid occurs [54]. This step occurs at a temperature above 167 °C and must be avoided due to toxicity and corrosiveness.

$$MgCl_2 \cdot 6\,H_2O \rightleftharpoons MgCl_2 \cdot 4\,H_2O + 2\,H_2O \tag{2.40}$$
$$MgCl_2 \cdot 4\,H_2O \rightleftharpoons MgCl_2 \cdot 2\,H_2O + 2\,H_2O \tag{2.41}$$
$$MgCl_2 \cdot 2\,H_2O \rightleftharpoons MgCl_2 \cdot H_2O + H_2O \tag{2.42}$$

The reaction enthalpy is for the reaction from magnesium chloride hexahydrate to the monohydrate is 252 kJ/mol with gaseous water and 76 kJ/mol with liquid water [46, 64]. The according theoretical energy density with gaseous water is 1945 MJ/m^3 and 374 kJ/kg with liquid water. The heat capacity is 1.55 kJ/(kg K) at 25 °C [19]. The melting point of magnesium chloride hexahydrate is 117 °C, which might lead to process difficulties due to phase change phenomena [54]. However, the main advantages of magnesium chloride are the low safety risks as no hazards have been classified. Moreover, low costs of only 117 €/kg (99.0-101.0% Emsure® ACS, ISO, Reag. Ph Eur) together with a great availability make $MgCl_2$ a promising storage medium [34]. According to the European Chemicals Agency (ECHA), $MgCl_2$ is manufactured in or imported to the European Economic Area at more than 10 kt/a [11]. Magnesium chloride hexahydrate is produced in large quantities as a by-product during potassium chloride production [54].

2.4.9 Strontium chloride

Strontium chloride hexahydrate is a potentially promising TCES material, due to its high energy density and full cyclability without chemical degradation in several heat storage applications. Moreover, $SrCl_2$ is used as an additive for $MgSO_4$ in TCES applications in order to improve the water vapour transfer and thus cycle stability [3]. The energy storage is based on the reaction given in (2.43).

$$SrCl_2 + 6\,H_2O \rightleftharpoons SrCl_2 \cdot 6\,H_2O + \Delta H_r \tag{2.43}$$

Thermal dehydration takes place in several steps with the occurrence of two intermediate states. First, the hexahydrate is dehydrated to the dihydrate at around 66 °C stated in (2.44). Upon further heating, the monohydrate is formed at 132 °C given in (2.45) [65]. The anhydrous salt is formed at a temperature of 320 °C, as given in (2.46). Thus, this reaction is not considered for this TCES application due to the limited suspension reactor conditions [26].

$$SrCl_2 \cdot 6\,H_2O \rightleftharpoons SrCl_2 \cdot 2\,H_2O + 4\,H_2O \tag{2.44}$$
$$SrCl_2 \cdot 2\,H_2O \rightleftharpoons SrCl_2 \cdot H_2O + H_2O \tag{2.45}$$
$$SrCl_2 \cdot H_2O \rightleftharpoons SrCl_2 + H_2O \tag{2.46}$$

The corresponding reaction enthalpy is 278 kJ/mol with gaseous water and 58 kJ/mol with liquid water [46]. Consequently, the theoretical energy storage density is 2030 MJ/m^3 with gaseous water and 220 kJ/kg with liquid water. The heat capacity is 0.30 kJ/(kg K) at 25 °C [19]. Apart from the good thermodynamic properties, the price for $SrCl_2 \cdot 6\,H_2O$ of 115 €/kg (ACS reagent, 99%) is still acceptable for a TCES medium, even though the availability of the anhydrous salt is relatively low with less than 1000 t/a in the European Economic Area [11, 37]. The salt $SrCl_2 \cdot 6\,H_2O$ is produced by dissolving strontium carbonate, obtained from the mineral strontianite or celestine, in diluted hydrochloric acid and subsequent crystallization [26]. Difficulties during the storage process might occur due to the low melting temperature of 100 °C and the necessity of additional safety measurements due to toxicity as well as the possibility for skin irritation and eye damage [44] [11].

2.4.10 Potassium oxalate

Potassium oxalate exists as a monohydrate and thus has the ability for thermochemical energy storage. Theoretical analyses indicated $K_2C_2O_4 \cdot H_2O$ as an alternative TCES material to calcium oxalate, despite showing a low energy storage density. The energy storage process is based on the reaction given in (2.47).

$$K_2C_2O_4 + H_2O \rightleftharpoons K_2C_2O_4 \cdot H_2O + \Delta H_r \tag{2.47}$$

The reaction enthalpy for this reaction is 56 kJ/mol with gaseous water and 13 kJ/mol with liquid water [64]. Accordingly, $K_2C_2O_4 \cdot H_2O$ has a theoretical energy density with gaseous water of 650 MJ/m^3 and an energy density with liquid water of 70 kJ/kg. The heat capacity is 0.25 kJ/(kg K) at 25 °C [19]. TGA measurements indicate two mass loss steps, which are ascribed to the dehydration at around 100-130 °C given in (2.48) and the decomposition at around 500-610 °C stated in (2.49) [41].

$$K_2C_2O_4 \cdot H_2O \rightleftharpoons K_2C_2O_4 + H_2O \tag{2.48}$$
$$K_2C_2O_4 \rightleftharpoons K_2CO_3 + CO \tag{2.49}$$

Potassium oxalate monohydrate crystallizes in a monoclinic crystal lattice [27]. Two polymorphic forms are known for the anhydrous salt, as at room temperature an orthorhombic crystal lattice is formed but the crystal structure of the high-temperature form is tetragonal [27]. Anhydrous potassium oxalate has a melting temperature of 397 °C, and potassium oxalate monohydrate is stable up to 130 °C, above decomposition occurs [41]. However, the potassium oxalate hydrate is expensive with more than 310 €/kg (ACS reagent, 99%) due to the complex and limited production [35]. It needs to be considered that potassium oxalate monohydrate causes serious eye irritation, is harmful if swallowed and causes skin irritation [11].

2.4.11 Calcium sulphate

Calcium sulphate is a potential TCES material, as it forms hydrates and the hydration reaction is theoretically reversible at low temperatures (<200°C) [21]. Thus suitable for the applied suspension reactor conditions. The TCES process relies on the reaction in (2.50).

$$CaSO_4 + 2\,H_2O \rightleftharpoons CaSO_4 \cdot 2\,H_2O + \Delta H_r \tag{2.50}$$

Calcium sulphate forms various hydrates, accordingly, the dehydration process itself takes place in two steps. First, the dihydrate is converted to the hemihydrate at 125-130 °C given in (2.51). In the second step, the anhydrous salt is obtained from the hemihydrate at 165 °C in (2.52) [67].

$$CaSO_4 \cdot 2\,H_2O \rightleftharpoons CaSO_4 \cdot 0.5\,H_2O + 1.5\,H_2O \tag{2.51}$$

$$CaSO_4 \cdot 0.5\,H_2O \rightleftharpoons CaSO_4 + 0.5\,H_2O \tag{2.52}$$

The reaction enthalpy for the dehydration of the dihydrate to the anhydrous salt is 101 kJ/mol with gaseous water and 13 kJ/mol with liquid water [64]. Accordingly, $CaSO_4 \cdot H_2O$ has a theoretical energy density with gaseous water of 1366 MJ/m^3 and an energy density with liquid water of only 78 kJ/kg. The heat capacity is 1.08 kJ/(kg K) at 25 °C [19]. However, calcium sulphate is considered to be safe, as no hazards have been classified [11]. Moreover, calcium sulphate is highly available at a low cost of only 120 €/kg (ReagentPlus®, ≥ 99%) [30]. According to the ECHA the salt is manufactured and imported to the European Economic Area with more than 10 Mt/a [11]. Calcium sulphate is produced in large quantities as a by-product in a number of processes such as flue-gas desulfurization [67].

2.4.12 Magnesium bromide

Magnesium bromide can form various hydrates and theoretical analyses indicate promising thermochemical energy storage potential [44, 62]. The storage process is based on the reaction in (2.53)

$$MgBr_2 + 6\,H_2O \rightleftharpoons MgBr_2 \cdot 6\,H_2O + \Delta H_r \tag{2.53}$$

The dehydration process of $MgBr_2 \cdot 6\,H_2O$ leads to three lower hydrates in overlapped temperature regions. First $MgBr_2 \cdot 4\,H_2O$ is obtained at 59-94 °C in (2.54), subsequently $MgBr_2{\cdot}2H_2O$ is formed at 88-107 °C in (2.55). The last utilized step from the dihydrate to the monohydrate takes place at 102-117°C in (2.56) [10]. Even higher temperatures lead to the formation of $MgOHBr \cdot n\,H_2O$ with $0 \leq n \leq 1.0$ in (2.57).

$$MgBr_2 \cdot 6\,H_2O \rightleftharpoons MgBr_2 \cdot 4\,H_2O + 2\,H_2O \tag{2.54}$$
$$MgBr_2 \cdot 4\,H_2O \rightleftharpoons MgBr_2 \cdot 2\,H_2O + 2\,H_2O \tag{2.55}$$
$$MgBr_2 \cdot 2\,H_2O \rightleftharpoons MgBr_2 \cdot H_2O + H_2O \tag{2.56}$$
$$MgBr_2 \cdot H_2O \rightleftharpoons MgOHBr \cdot n\,H_2O\ (0 \leq n \leq 1.0) \tag{2.57}$$

The reaction enthalpy for this reaction is 435 kJ/mol with gaseous water and 171 kJ/mol with liquid water [46, 64]. The according theoretical energy density with gaseous water is 2976 MJ/m^3 and 584 kJ/kg with liquid water. The heat capacity is 0.2 kJ/(kg K) at 25 °C [19]. Magnesium bromide can cause serious eye, skin and respiratory irritation [11]. Additionally, the salt has a low availability and is rather expensive with 240 €/kg (99%) [33].

2.4.13 Manganese sulphate

Manganese sulphate might be a promising TCES material as it can form several hydrates. However, there is no literature available on energy storage properties. The storage process is based on the reaction given in (2.58)

$$MnSO_4 + 4\,H_2O \rightleftharpoons MnSO_4 \cdot 4\,H_2O + \Delta H_r \tag{2.58}$$

The dehydration reaction of $MnSO_4 \cdot 4\,H_2O$ proceeds over several steps, though different dehydration mechanisms have been reported in the literature. Most likely, $MnSO_4 \cdot 4\,H_2O$ is first dehydrated to the trihydrate in (2.59) [55]. Subsequently, the dihydrate in (2.60) and the monohydrate in (2.61) are formed. Theoretically, all these reaction steps occur below 170 °C [55]. The last dehydration step from $MnSO_4 \cdot H_2O$ to the anhydrous salt in (2.62) takes place at a temperature over 340°C and thus is not considered for this storage application [55].

$$MnSO_4 \cdot 4\,H_2O \rightleftharpoons MnSO_4 \cdot 3\,H_2O + H_2O \tag{2.59}$$
$$MnSO_4 \cdot 3\,H_2O \rightleftharpoons MnSO_4 \cdot 2\,H_2O + H_2O \tag{2.60}$$
$$MnSO_4 \cdot 2\,H_2O \rightleftharpoons MnSO_4 \cdot H_2O + H_2O \tag{2.61}$$
$$MnSO_4 \cdot H_2O \rightleftharpoons MnSO_4 + H_2O \tag{2.62}$$

The reaction enthalpy for the reaction of manganese sulphate tetrahydrate to monohydrate is 156 kJ/mol with gaseous water and 24 kJ/mol with liquid water [46, 64]. The according theoretical energy density with gaseous water is 2064 MJ/m^3 and 108 kJ/kg with liquid water. The heat capacity is 0.2 kJ/(kg K) at 25 °C [19]. Unfortunately, manganese sulphate and all hydrates can cause damage to organs through prolonged or repeated exposure and are toxic to aquatic life [11]. Manganese sulphate costs about 300 €/kg (>95%) and is manufactured or imported to the European Economic Area with more than 10 kt/a, which indicates medium availability [11, 59].

3 Applied principles and methods

In this chapter the applied principles of this thesis and methods are described. The experimental setup and essential calculations are explained in detail. Moreover, the reaction conditions of each material system are stated.

3.1 Materials

Hydrogenated mineral oil based heat transfer fluid Fragoltherm® Q-32-N, and polydimethylsiloxane based heat transfer fluid Fragoltherm® X-400-A were purchased from Fragol AG (Muelheim an der Ruhr, Germany). Rapeseed oil was purchased from Patrick Schlichter Hofgut (Bad Liebenzell, Germany). The salts magnesium sulphate heptahydrate ($MgSO_4 \cdot 7\,H_2O$) and magnesium chloride hexahydrate ($MgCl_2 \cdot 6\,H_2O$) were purchased from Dicleanshop (Dortmund, Germany). Potassium sulphate (K_2SO_4), zinc sulphate heptahydrate ($ZnSO_4 \cdot 7\,H_2O$), di-potassium oxalate hydrate ($K_2C_2O_4 \cdot H_2O$) and manganese sulphate tetrahydrate ($MnSO_4 \cdot 4\,H_2O$) were purchased from Merck (Darmstadt, Germany). Iron sulphate heptahydrate ($FeSO_4 \cdot 7\,H_2O$), aluminium sulphate octadecahydrate ($Al_2(SO_4)_3 \cdot 18\,H_2O$), magnesium bromide hexahydrate ($MgBr_2 \cdot 6\,H_2O$) and calcium sulphate dihydrate ($CaSO_4 \cdot 2\,H_2O$) were purchased from Sigma Aldrich (Darmstadt, Germany). Molecular sieves (zeolite) 4A, 0.4-0.8 mm beads, were purchased from abcr GmbH (Karlsruhe, Germany). Strontium chloride hexahydrate, min. 99% ($SrCl_2 \cdot 6\,H_2O$) was purchased from S3 Handel und Dienstleistungen UG (Bad Oeynhausen, Germany). Copper sulphate pentahydrate ($CuSO_4 \cdot 5\,H_2O$) was purchased from Carl Roth GmbH + Co. KG (Karlsruhe, Germany).

3.2 Synthesis of Tutton's salts

In general, Tutton's salts $K_2M(SO_4)_2 \cdot 6\,H_2O$ ($M = Zn, Mg, Cu$) are synthesised by first dissolving stoichiometric amounts of K_2SO_4 and $MSO_4 \cdot x\,H_2O$ (1:1) in deionised water. Additional heating is applied to increase the solubility. As soon as the educts are completely dissolved, the temperature is reduced to room temperature. Through slow evaporation of the water, crystals are formed. The crystallisation process can be accelerated by heating the solution and thus evaporating water. The crystals are retrieved from the solution via vacuum filtration followed by a washing step with acetone [56].

In more detail, $K_2Zn(SO_4)_2 \cdot 6\,H_2O$ was synthesised by evaporating an aqueous solution of equimolar amounts of $ZnSO_4 \cdot 7\,H_2O$ and K_2SO_4. Likewise, $K_2Mg(SO_4)_2 \cdot 6\,H_2O$ was synthesised from an aqueous equimolar solution of $MgSO_4 \cdot 7\,H_2O$ and K_2SO_4. The resulting

crystals were recovered from the solution by vacuum filtration and washed with acetone. The particles were crushed into fine powder in a mortar. $K_2Cu(SO_4)_2 \cdot 6\,H_2O$ was synthesized with the same procedure by dissolving equimolar amounts of $CuSO_4{\cdot}7H_2O$ and K_2SO_4, but the evaporation process must be conducted slowly to achieve high yields. Fast evaporation leads to the formation of a green side product $KCu_2(SO_4)_2[(OH)(H_2O)]$ [47].

3.3 Experimental setup three-neck flask

Innovative reaction systems were tested preliminary in a three-neck flask setup in order to get first information regarding the reaction conditions. Particularly, the reaction temperature and reaction enthalpy as well as behaviour of the material during dehydration and rehydration itself (e.g.: foaming and agglomeration) are investigated. The experimental setup can be seen in the figure 3.1 and contains a three-neck flask as the central component, a vertical cooler placement together with a water collector and a mechanical stirrer. The heating unit consists of a heating plate and a oil bath. Additionally a nitrogen gas inlet and a thermocouple (RS Pro Inconel Thermocouple Typ K) together with a thermometer (RS Pro Digital Thermometer Typ K) are connected to the system.

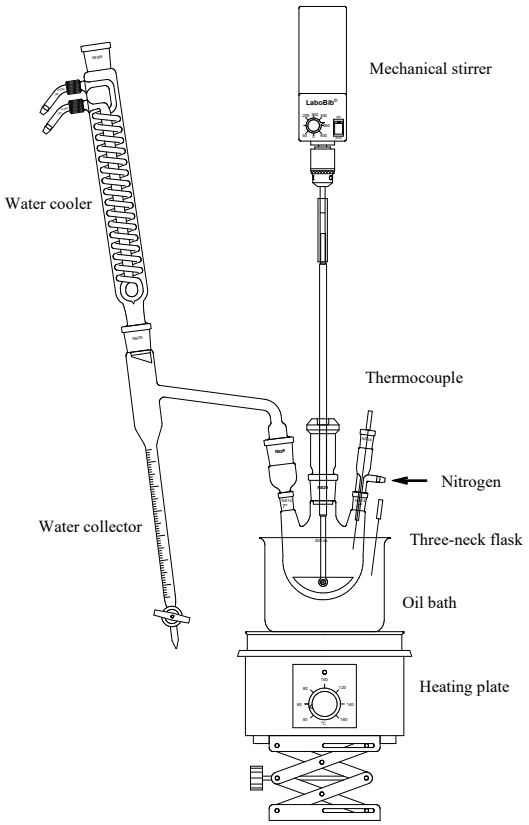

Figure 3.1: Three-neck flask setup for preliminary experiments

During the charging process, the heating of the system is done with the oil bath, while the gradual temperature rise is monitored manually. Dehydration reaction takes places and consequently water is evaporated. The evaporated water is condensed with the cooler and collected in the water collector to measure the amount and consequently calculating the conversion of the reaction. The nitrogen flow is applied to the system to support evaporation and vapour transport. After the system is cooled to room temperature again, the discharging process is conducted. A specific amount of water is added to the system with a syringe at a speed of 0.2 mL/min. The rehydration reaction leads to a temperature rise which is monitored manually for further calculations.

3.4 Experimental setup reactor

The screening of promising gas-solid reaction systems for thermochemical energy storage were carried out in a up-scaled reactor. The experimental setup is depicted in figure 3.2 and features a double-walled reactor as the central component. Similar to the three-neck flask setup, the setup contains a vertical cooler placement together with a water collector and a mechanical stirrer. Heating is performed with a heating bath circulation thermostat (Huber CC-308B). A nitrogen gas inlet and a thermocouple (RS Pro Inconel Thermocouple Typ K) together with a thermometer (RS Pro Digital Thermometer Typ K) are connected to the system as well.

The suspension is heated according to a specific temperature program adapted to every system individually. Temperature inside the reactor is monitored with the help of the thermocouple together with the thermometer. Consequently, the dehydration reaction takes place, and water is evaporated. In order to enhance evaporation efficiency, the nitrogen stream with 0.2 L/min is added to the setup, which helps to transport the vapour from the reactor to the cooler. Subsequently, the water is condensed and the volume in the water collector measured. The amount of condensed water indicates the conversion of the reaction calculated based on the theoretical stoichiometric water in the system. Once the reactor with the suspension is cooled down to room temperature, the discharging reaction is conducted. During the rehydration reaction water is added with 0.2 ml/s, resulting a change in temperature, which is measured with a resistance thermometer. Subsequently, the specific reaction enthalpy can be calculated.

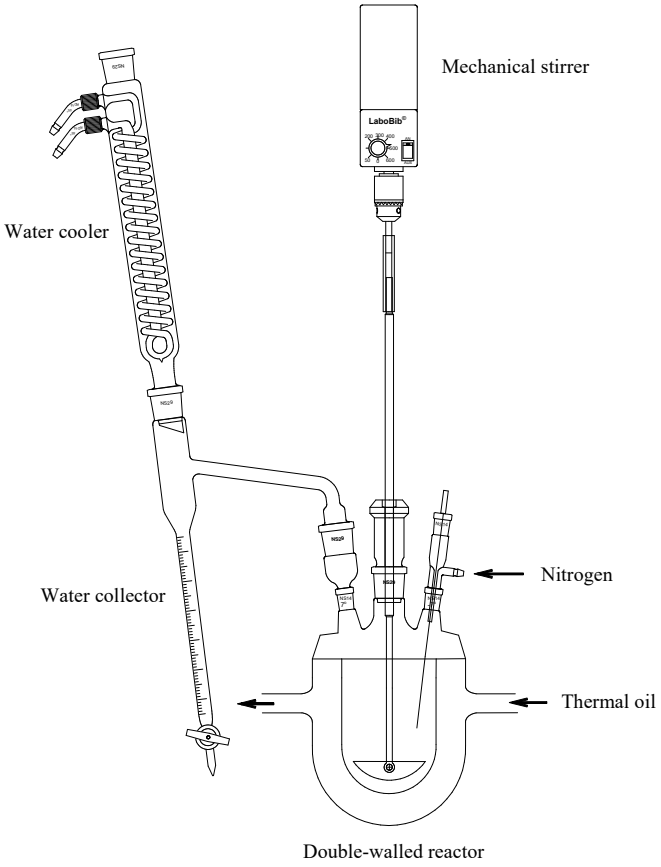

Figure 3.2: Up-Scaled reactor experimental setup for the screening of promising materials

3.5 Data evaluation

During the dehydration and rehydration reaction important parameters are characterised. On the one hand, these parameters give significant information about the process itself, on the other hand, are essential for the calculation of further characteristics. One of the most important parameters measured during all reaction steps is the temperature. The thermocouple allows for continuously tracking of the temperature inside the reaction zone.

During charging the start of the dehydration reaction is determined visually based on the start of water condensation and the prevailing temperature T_{dehyd} noted. The volume of collected water is another significant parameter of the dehydration reaction as it gives information regarding the conversion based on (3.1).

$$X_i = \frac{V_c(H_2O)}{V_s(H_2O)} \tag{3.1}$$

The volume of condensed water V_c is divided by the stoichiometric volume V_s leading to the conversion X_i.

During the discharging process the reaction enthalpy is released again. The resulting temperature increase ΔT allows the calculation of the heat transferred to the solid educt Q_{educt} in (3.2), the thermal oil $Q_{thermal\ oil}$ in (3.3) and additional water in the system $Q_{water,\lambda>1}$ in (3.4).

$$Q_{educt_{(s)}} = m_{educt_{(s)}} \cdot \Delta T \cdot \overline{c}_{p_{educt_{(s)}}} \tag{3.2}$$

$$Q_{thermal\ oil_{(l)}} = m_{thermal\ oil_{(l)}} \cdot \Delta T \cdot \overline{c}_{p_{thermal\ oil_{(l)}}} \tag{3.3}$$

$$Q_{water,\lambda>1_{(s)}} = m_{water,\lambda>1_{(l)}} \cdot \Delta T \cdot \overline{c}_{p_{water_{(l)}}} \tag{3.4}$$

The transferred heat Q is calculated based on the mass of the substance m, the temperature change ΔT and the specific heat capacity $\overline{c}_p$ at standard conditions. $\lambda > 1$ indicates overstoichiometric amount of water in the system during the rehydration reaction. It needs to be considered for the heat transfer, as it does not react with the solid material. Subsequently, the experimental energy storage density $\Delta h_{m,exp.}$ can be calculated as shown in (3.5).

$$\Delta h_{m,exp.} = \frac{Q_{educt_{(s)}} + Q_{thermal\ oil_{(l)}} + Q_{water,\lambda>1_{(l)}}}{m_{educt_{(s)}}} \tag{3.5}$$

The sum of the heat transferred to the solid educt Q_{educt}, the thermal oil $Q_{thermal\ oil}$ and additional water in the system $Q_{water,\lambda>1}$ are divided by the educts mass $m_{educt_{(s)}}$, resulting in the experimental energy storage density $\Delta h_{m,exp.}$.

3.6 Reaction conditions

Reaction conditions for each material system are explained in detail in the following section. Particularly, the suspension medium, solid to oil ratio and applied temperature profile during charging as well as the amount and speed of added water for the discharging process are stated.

3.6.1 Magnesium sulphate reaction conditions

$MgSO_4 \cdot 7\,H_2O$ was tested in three different suspension mediums, mineral oil, silicone oil and rapeseed oil. 30 wt.% of salt hydrate in the various oils were used in all runs. The experiment was carried out according to the described procedure above and the material system was tested for several runs to determine cycle stability. Two different temperature

programs were applied. Program 1 consisted of a heating ramp from RT to 100 °C in 15 min followed by a second heating ramp to 120 °C in 67 min. Program 2 consisted of a heating ramp from RT to 150 °C with 10 °C/min. Dehydration experiments were conducted under nitrogen flow (0.2 L/min) in order to support dehydration and transport of vapor to the cooler. For rehydration the exact amount of beforehand condensed water was added to the system with 0.2 mL/min.

3.6.2 Zinc sulphate reaction conditions

Experiments with the material system $ZnSO_4 \cdot 7\,H_2O$ were carried out in mineral oil, rapeseed oil and silicone oil. In the three-neck flask a suspension of 25 wt.% salt hydrate in oil were used, but in the up-scaled reactor 30 wt.% of salt were used. $ZnSO_4 \cdot 7\,H_2O$ was crushed into fine powder in a mortar before usage. Experiments followed the procedure describe above, however, two different temperature programs were applied. Temperature program 1 consisted of a first heating ramp up to 100 °C with 5 °C/min and a subsequent heating ramp up to 140 °C with 0.3 °C/min. Temperature program 2 consists again of a heating ramp up to 100 °C with 5 °C/min and a subsequent temperature ramp up to 150 °C with 0.3 °C/min. The salt was discharged by adding stoichiometric amount of water to the system with 0.2 mL/min. Moreover, the material was tested up to 5 runs to ensure cyclability. The suspension was stirred with 200 rpm in the three-neck flask setup and with 300 rpm in the up-scaled reactor.

3.6.3 Iron sulphate reaction conditions

$FeSO_4 \cdot 7\,H_2O$ suspended in mineral oil and silicone oil was tested preliminary in the three-neck flask setup to get more information regarding the reaction behaviour of the system, followed by large scale tests in the reactor. In all cases the suspension was heated to 150 °C directly (10 °C/min in the reactor). The suspension consisted of 25 wt.% salt hydrate. Stoichiometric amount of water was added dropwise (0.2 mL/s) to the system for discharging. Again, the suspension was stirred with 200 rpm in the three-neck flask setup and with 300 rpm in the up-scaled reactor.

3.6.4 Aluminium sulphate reaction conditions

$Al_2(SO_4)_3 \cdot 18\,H_2O$ was crushed into fine powder in a mortar before experiments. 25 wt.% of the material were suspended in mineral oil. Experiments were conducted in the three-neck flask setup and the suspension heated up to 170 °C stepwise to get information on possible occurring hydrate levels. Discharging was performed by adding the stoichiometric amount of water dropwise (0.2 mL/s) to the system. The suspension was stirred with 200 rpm.

3.6.5 Potassium zinc sulphate reaction conditions

30 wt.% of the salt hydrate $K_2Zn(SO_4)_2 \cdot 6\,H_2O$ were suspended in mineral oil. Following the suspension was first heated up to 120 °C (10 °C/min), subsequently stepwise increased up to 155 °C while being stirred with 300 rpm. After the suspension was cooled to room temperature again, stoichiometric amount of water was added dropwise (0.2 mL/s) for discharging.

3.6.6 Potassium magnesium sulphate reaction conditions

$K_2Mg(SO_4)_2 \cdot 6\,H_2O$ suspended in mineral oil with 30 wt.% and first heated up to 120 °C with 10 °C/min for dehydration reaction. The temperature was subsequently increased up to 160 °C until the reaction seemed to be completed as no more water was condensed. For rehydration (discharging) stoichiometric amount of water was added dropwise (0.2 mL/s) to the suspension. Stirring with 300 rpm was applied to the suspension.

3.6.7 Potassium copper sulphate reaction conditions

Fine powder of $K_2Cu(SO_4)_2 \cdot 6\,H_2O$ was suspended in mineral oil (30 wt.% of salt hydrate). First, the suspension was heated up to 100 °C with 3.75 °C/min and subsequently increased up to 150 °C with 0.5 °C/min and hold until the reaction seemed to be completed as no more water was condensed. The suspension was stirred with 300 rpm. For rehydration (discharging) stoichiometric amount of water was added dropwise (0.2 mL/s) to the suspension.

3.6.8 Strontium bromide reaction conditions

$SrBr_2 \cdot 6\,H_2O$ was tested in the three-neck flask prior to up-scaled experiments in the reactor. 30 wt.% of the salt hydrate were suspended in mineral oil. The suspension was heated up 150 °C with 10 °C/min and hold until reaction seemed to be completed, subsequently increased to 160 °C to ensure full conversion. For discharging (rehydration) water was added with 0.2 mL/s to the suspension and the accompanying temperature lift recorded. During the experiment the suspension was stirred with 300 rpm.

3.6.9 Zeolite reaction conditions

Zeolite 4A suspended in mineral oil (25 wt.% salt hydrate) was tested in the three-neck flask setup for preliminary experiments. The temperature profile applied to the suspension consisted of a stepwise increase up to 160 °C while stirring with 200 rpm. Subsequent discharging was performed by adding water (0.2 mL/s) to the suspension.

3.6.10 Magnesium chloride reaction conditions

$MgCl_2 \cdot 6\,H_2O$ was tested in the three-neck flask setup with a salt hydrate to mineral oil ratio of 25 wt.%. The temperature was gradually increased up to 180 °C for dehydration while stirring the suspension at 200 rpm. Subsequently, discharging was performed by adding the stoichiometric amount of water (0.2 mL/s) to the stirred suspension.

3.6.11 Strontium chloride reaction conditions

Due to promising preliminary tests in the three-neck flask setup, $SrCl_2 \cdot 6\,H_2O$ was tested in the up-scaled reactor. The salt was suspended in mineral oil with a salt hydrate to oil ratio of approx. 30 wt.% (75 g $SrCl_2 \cdot 6\,H_2O$, 175 g mineral oil) and heated stepwise up to 170 °C for dehydration. The temperature program starts with heating to 110 °C with 5 °C/min, followed by heating up to 170 °C/min with 0.5 °C/min. Subsequent discharging was performed by adding water (0.2 mL/s) to the suspension while recording the temperature increase. During the whole experiment the suspension was stirred with 300 rpm.

3.6.12 Di-Potassium oxalate reaction conditions

Di-Potassium oxalate hydrate was tested in the three-neck flask setup. 25 wt.% of the salt $K_2C_2O_4 \cdot H_2O$ were suspended in mineral oil and stepwise heated up to 130 °C under nitrogen flow as well as stirring with 200 rpm. Subsequently, the suspension was rehydrated by adding water (0.2 mL/s) while recording the temperature increase.

3.6.13 Calcium sulphate reaction conditions

Calcium sulphate dihydrate suspended in mineral oil was tested in the three-neck flask setup with 25 wt.% salt hydrate in mineral oil. The temperature was gradually increased up to 160 °C under nitrogen flow for dehydration and stirring of 200 rpm. Following, discharging was performed by adding stoichiometric amount of water (0.2 mL/s) to the suspension.

3.6.14 Magnesium bromide reaction conditions

Magnesium bromide hexahydrate was tested in the three-neck flask setup for several runs. 25 wt.% of the salt hydrate were suspended in mineral oil and stepwise heated up to 200 °C for the charging reaction. For discharging, stoichiometric amounts of water was added to the system with 0.2 mL/s.

3.6.15 Manganese sulphate reaction conditions

Manganese sulphate tetrahydrate (25 wt.%) suspended in mineral oil was tested in the three-neck flask setup. The suspension was heated up to 210 °C stepwise and stirred at 200 rpm. No rehydration experiments were performed.

4 Results and Discussion

In this chapter the experimental results of all investigated systems are evaluated and discussed in detail. During the charging process, the conversion and dehydration temperature were determined and assessed closely. Additionally, the temperature increase and corresponding energy output during the discharging reaction are stated and consequently evaluated. Particular attention was paid to side effects like agglomeration, phase change, and foaming.

4.1 Magnesium sulphate

Charging

$MgSO_4 \cdot 7\,H_2O$ is theoretically a promising material for TCES as it has a high storage density, high theoretical specific reaction enthalpy, and is safe to handle, as already described in more detail in chapter 2.4.1. The system $MgSO_4 \cdot 7\,H_2O$ was tested in three different suspension mediums, mineral oil, silicone oil, and rapeseed oil. In figure 4.1 the experimental results of $MgSO_4 \cdot 7\,H_2O$ in silicone oil are shown.

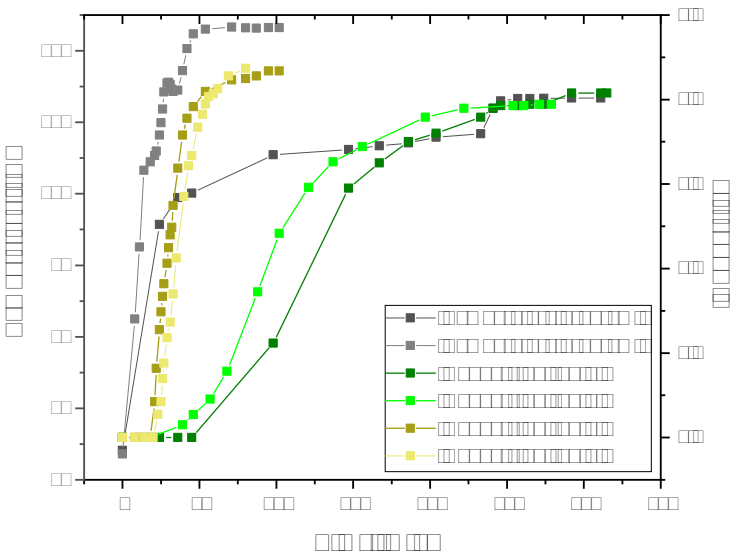

Figure 4.1: Experimental results for the charging reaction of $MgSO_4 \cdot 7\,H_2O$ in silicone oil

Two different temperature programs were applied to the system, which can be seen in the graph. The conversion is between 79% to 88% in all runs, depending on the applied temperature program. In run 1.1 a conversion of 82% is reached, which decreased to 79% in the following run. In run 2.1 and run 2.2 the conversion is 88%. The time needed to reach maximum conversion strongly depends on the applied temperature profile. Fast heating in temperature program 2 ensures high conversion in a short time of about 1.5 h. In comparison, temperature program 1 needs about 5 h to reach the maximum conversion. The conversion of run 1.1 is slightly decreasing in the second cycle 1.2 by approximately 3%, which indicates, that the material might not be stable for several cycles. The temperature at the beginning of the dehydration reaction is between 100 to 110 °C for all four runs, again varying a bit with the applied temperature profile. Unfortunately, agglomeration occurred during the reaction, leading to a termination of the whole storage process after only two cycles as stirring was not possible anymore. A possible explanation for the occurrence of this phenomenon might be the low melting temperature of $MgSO_4 \cdot 7\,H_2O$ of only 52.5 °C [63]. One might think slower heating is a solution to overcome this problem as the material can fully dehydrate before melting, but no differences in agglomeration depending on the used temperature profile were observed.

Similar results can be seen for the experimental outcome of $MgSO_4 \cdot 7\,H_2O$ in rapeseed oil. In figure 4.2 the charging process, including temperature profile and conversion depending on time are depicted.

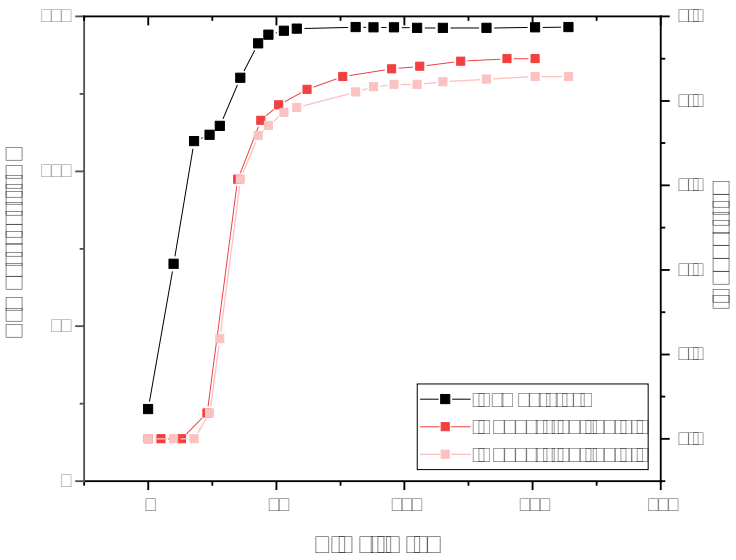

Figure 4.2: Experimental results for the charging reaction of $MgSO_4 \cdot 7\,H_2O$ in rapeseed oil for two runs

Two runs of $MgSO_4 \cdot 7\,H_2O$ in rapeseed oil were conducted, reaching a conversion of 90% in the first run but only 86% in the second run. The temperature at the beginning of the dehydration reaction of 110 °C is the same for both runs. The dehydration reaction

takes about 2.5 h, but as mentioned above strongly depends on the temperature program in general. Unfortunately, agglomeration occurred also in rapeseed oil leading to a termination of the process after the second run. Thus, the experiment of $MgSO_4 \cdot 7\,H_2O$ in rapeseed oil was stopped after the two given runs.

The third tested suspension medium was mineral oil. The results of the charging process, including conversion and the temperature profile are shown in figure 4.3.

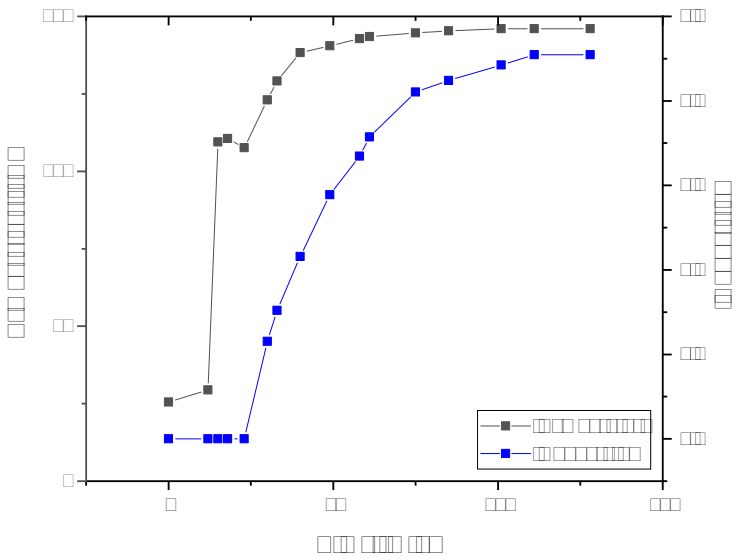

Figure 4.3: Experimental results for the charging reaction of $MgSO_4 \cdot 7\,H_2O$ in mineral oil

The achieved conversion of the dehydration reaction in mineral oil is 91%. The dehydration reaction started at a temperature of 105 °C and lasted for about 2 h. However, the main problem was severe agglomeration, which led to a termination of the process after the first dehydration phase. Therefore, no further experiments were conducted with $MgSO_4 \cdot 7\,H_2O$ in mineral oil.

In figure 4.4 a comparison of the salt in all three tested suspension media is depicted. Exemplary plots of each system including temperature profile and conversion depending on time are shown. In general, after a small preheating phase at the beginning, the dehydration reaction starts which can be seen by a steady increase in conversion. Further increase in temperature leads to a higher conversion as the reaction prolongs. The reaction process over time is similar in all suspension media. The average temperature of dehydration is around 105 °C for all systems. The conversion of $MgSO_4 \cdot 7\,H_2O$ in mineral oil is 91%. The timescale of dehydration is around 2 h. Followed by an average conversion in rapeseed oil of 88% and a time of dehydration of about 2.5 h. The average conversion in silicone oil is even lower with only 84% in about 2.5 h. It has to be mentioned that the time of dehydration strongly depends on the heating rate.

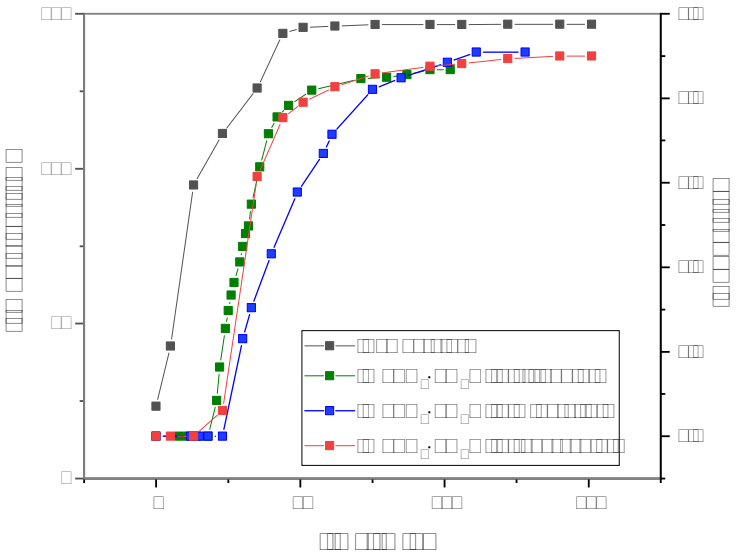

Figure 4.4: Experimental results for charging reaction of $MgSO_4 \cdot 7\,H_2O$ in different suspension media

The slight differences in conversion and reaction time between the different oils might be explained by agglomeration, physical properties of the oil, or measurement inaccuracy due to the relatively small number of experiments. Apart from that, the setup is not accurate enough to interpret a deviation of 3%. The obtained results regarding conversion indicate that mineral oil is the most promising suspension medium for $MgSO_4 \cdot 7\,H_2O$, followed by rapeseed oil. There are indications, that the conversion is decreasing with each cycle. However, the main difficulty of $MgSO_4 \cdot 7\,H_2O$ is the occurrence of agglomeration during dehydration. The strongest agglomeration appeared in mineral oil, followed by silicone and rapeseed oil. This is a slight contradiction to the conversion results, but might be due to the small number of experiments. Agglomeration of small particles reduces the availability of reaction sites and therefore influences conversion and the following discharging (rehydration) process negatively. Moreover, severe agglomeration can eventually cause a total collapse of the storage process as stirring of the suspension is not possible anymore. Consequently, agglomeration is a big problem that needs to be solved.

Discharging

Specific reaction enthalpy of the discharging reaction was calculated from the increase in temperature in equation (3.5). The temperature increase during the discharging reaction of $MgSO_4 \cdot H_2O$ in silicone oil is shown in figure 4.5.

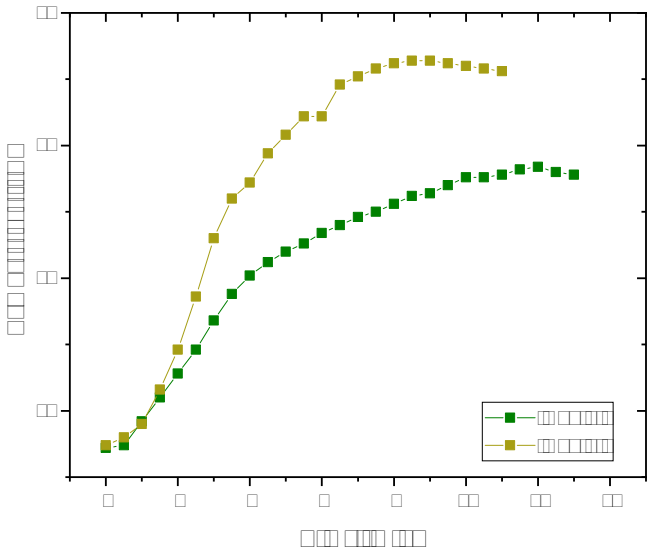

Figure 4.5: Experimental results for the discharging reaction of $MgSO_4 \cdot H_2O$ in silicone oil

Only the experimental results of the discharging reaction of run 1.1 and 2.1 are plotted, since the second cycle of each experiment had to be stopped before discharging due to agglomeration, as mentioned above. The temperature increased about 10.6 °C in run 1.1 and 14.5 °C in run 2.1 which corresponds to an experimental energy output of 54 kJ/kg and 74 kJ/kg (losses not included). It takes 10-12 minutes to reach the maximum temperature, which gives an indication of the kinetics of the reaction.

The results of the discharging process of $MgSO_4 \cdot H_2O$ in rapeseed oil are depicted in figure 4.6. Again the temperature increase was measured and the corresponding energy output calculated. In the first run 1.1 the temperature increased by 11.2 °C but only 4.7 °C in the second run 1.2. This corresponds to an experimental energy output of 78 kJ/kg and 40 kJ/kg. The decrease from run 1.1 to run 1.2 can be explained by the occurrence of advanced agglomeration. However, it takes again 10-12 minutes to reach the maximum temperature.

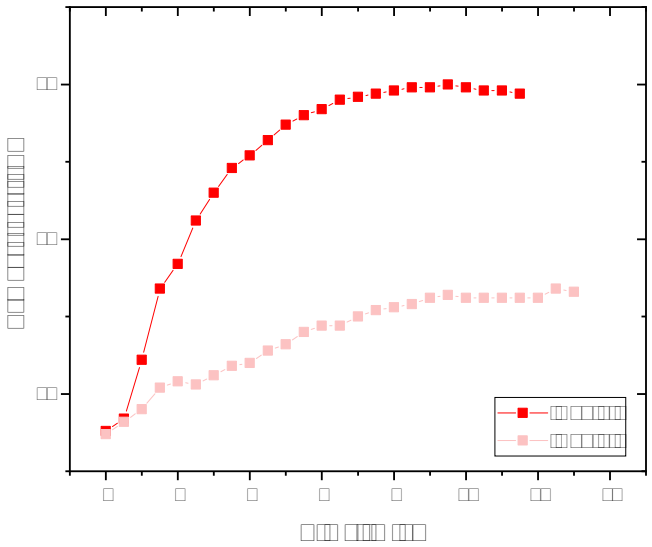

Figure 4.6: Experimental results for the discharging reaction of $MgSO_4 \cdot H_2O$ in rapeseed oil

In figure 4.7 a comparison with exemplary curves for the temperature rise over time during the discharging reaction of $MgSO_4 \cdot H_2O$ in silicone and rapeseed oil is shown. No results for $MgSO_4 \cdot H_2O$ in mineral oil are given.

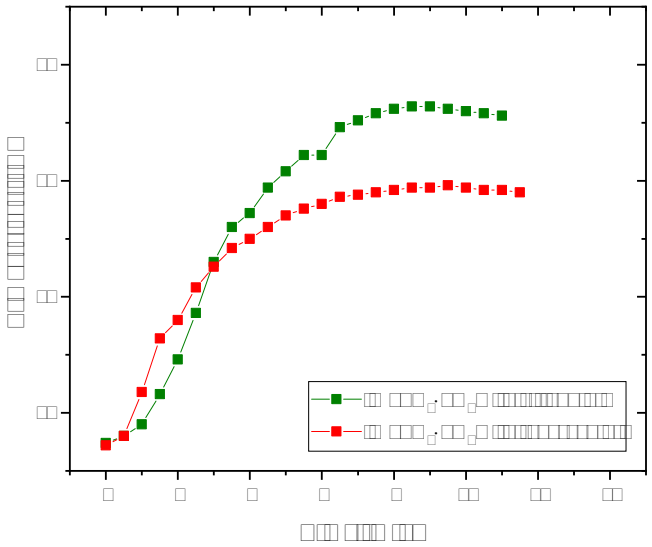

Figure 4.7: Experimental results for the discharging reaction of $MgSO_4 \cdot H_2O$ in different suspension media

The temperature rise for $MgSO_4 \cdot H_2O$ in silicone oil is higher than for $MgSO_4 \cdot H_2O$ in rapeseed oil. The temperature rise for the system $MgSO_4 \cdot H_2O$ in mineral oil could not be determined due to agglomeration. However, all values show uncertainty due to the occurrence of agglomeration. The greater the agglomeration, the lower the temperature rise and thus specific reaction enthalpy. This can be explained by the reduction of active surface area. The highest achieved specific reaction enthalpy is 78 kJ/kg with liquid water. These experimental results show a promising trend but there is still potential for improvement compared to the theoretical value of 260 kJ/kg. Nevertheless, the main disadvantage of the system is agglomeration which needs to be solved in order to reliably use the material for thermochemical energy storage applications.

4.2 Zinc sulphate

Charging

The storage material $ZnSO_4 \cdot 7\,H_2O$ was tested in three different suspension media, mineral oil, rapeseed oil, and silicone oil. Again, the conversion is calculated from the measured volume of condensed water. In figure 4.8 the experimental results, including an exemplary temperature profile and conversion depending on time, of $ZnSO_4 \cdot 7\,H_2O$ in mineral oil are shown in figure 4.8.

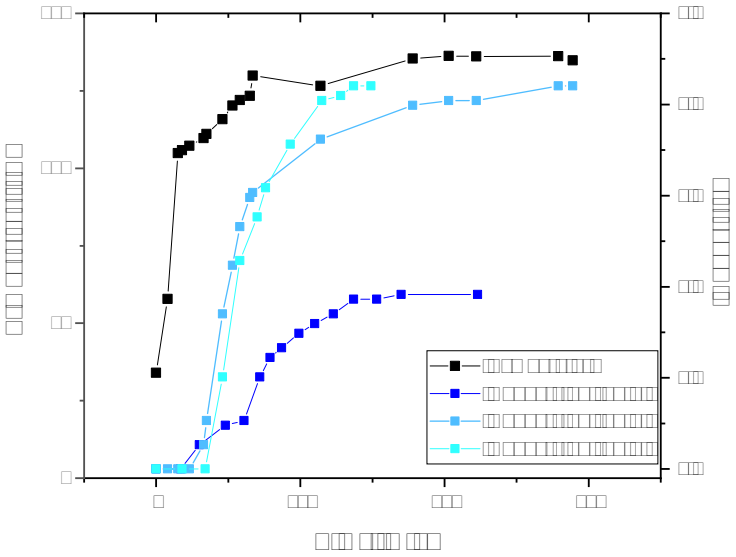

Figure 4.8: Experimental results for the charging reaction of $ZnSO_4 \cdot 7\,H_2O$ in mineral oil

During the charging of the first run 1.1 a conversion of only 38% was achieved, however, the second 1.2 and third run 1.3 reached 84%. The conversion in run 1.1 is much lower than the conversion of run 1.2 and 1.3. A possible reason for this is the stoichiometric

addition of water during the rehydration reaction and thus the accumulation of water in the process. Another reason could be, that the starting material was already dehydrated to a certain degree. The dehydration started at a temperature of about 105 °C and lasted for about 2.5-4.5 h in all runs. A reason for the overall low conversion might be agglomeration, which increased with each cycle and caused the termination of the storage process after three cycles. The occurrence of agglomeration can be explained with the low melting point of 100 °C of $ZnSO_4 \cdot 7\,H_2O$ [48].

The salt $ZnSO_4 \cdot 7\,H_2O$ was also tested in rapeseed oil as suspension medium. The experimental results, including the conversion and temperature profile are shown in figure 4.9.

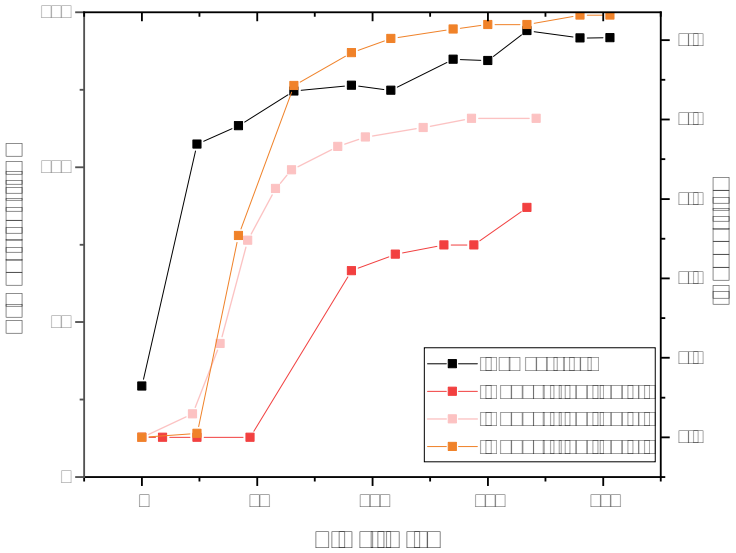

Figure 4.9: Experimental results for the charging reaction of $ZnSO_4 \cdot 7\,H_2O$ in rapeseed oil for several runs

The conversion in rapeseed oil is only 60% at run 1.1, 80% at run 1.2, and more than 100% at run 1.3. This can again be explained by the stoichiometric addition of water to the system and thus accumulation. Therefore no conclusion about cycle stability can be drawn. The dehydration started at around 105 °C in all runs and lasted for about 3 h. Unfortunately, agglomeration occurred, which influenced the results negatively.

The third tested suspension medium was silicone oil. In figure 4.10 the conversion over time and an exemplary temperature profile are shown. The conversion of the discharging reaction of $ZnSO_4 \cdot 7\,H_2O$ in silicone oil is 82%. Due to agglomeration, only one run was possible. The dehydration reaction started at 105 °C and lasted for 3 h.

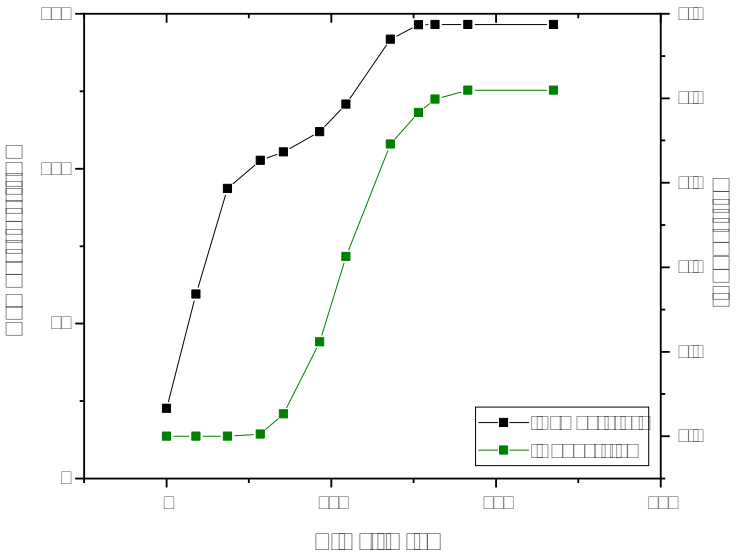

Figure 4.10: Experimental results for the charging reaction of $ZnSO_4 \cdot 7\,H_2O$ in silicone oil

A comparison of the three suspension media used for the storage process of zinc sulphate gives more information. In figure 4.11 the conversion over time and an exemplary temperature profile are shown for every system.

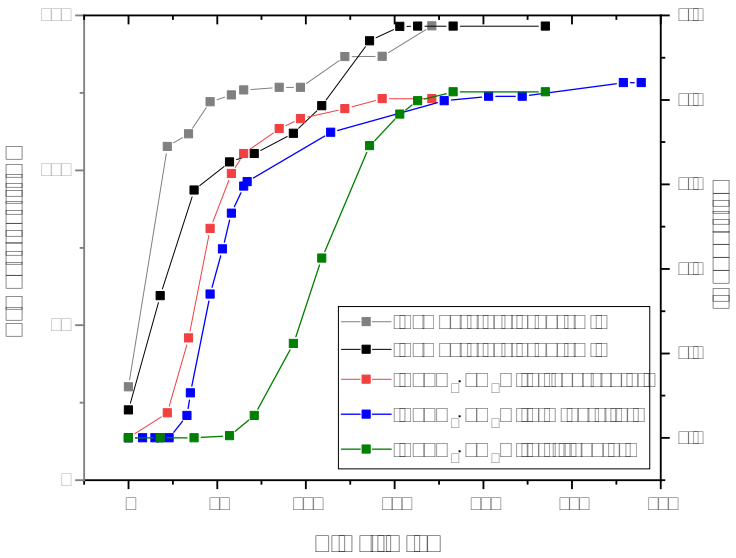

Figure 4.11: Experimental results for the charging reaction of $ZnSO_4 \cdot 7\,H_2O$ in three different suspension media

$ZnSO_4 \cdot 7\,H_2O$ is expected to achieve similar results as the system $MgSO_4 \cdot 7\,H_2O$, as it also has a high theoretical specific reaction enthalpy and only slightly lower energy storage density. The material system was tested in three different suspension media for several runs. The dehydration temperature of 105 °C is the same for all systems, nevertheless, time needed for complete dehydration is higher for $ZnSO_4 \cdot 7\,H_2O$ in mineral oil, but strongly depends on the applied temperature profile. Conversion is about the same for all suspension media. No conclusion about cycle stability can be drawn, as a stoichiometric amount of water was added to the system which accumulated. However, agglomeration is hindering good cycle stability. Moreover, conversion is lower than theoretically expected and the dehydration process takes longer as the transport of water vapour through the material is restricted. At around 100 °C a phase change was visible in all runs, which might be the reason for the agglomeration. This assumption is supported by fact that $ZnSO_4 \cdot 7\,H_2O$ has a melting temperature of 100 °C [48].

Discharging

Experimental discharging by adding water led to a temperature increase which was measured. In figure 4.12, the temperature profile during the dehydration reaction of $ZnSO_4 \cdot H_2O$ in mineral oil for three runs is given.

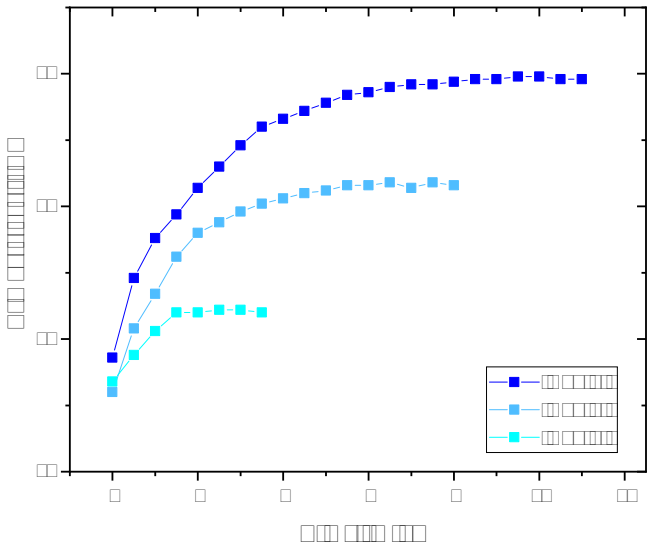

Figure 4.12: Experimental results for discharging of $ZnSO_4 \cdot H_2O$ in mineral oil

The temperature increased by 10.5 °C in run 1.1, slightly less in run 1.2 (7.9 °C), and only about 2.7 °C in run 1.3. The reason for this is most likely agglomeration, as the availability of reaction sites is reduced. The temperature increase corresponds to specific reaction enthalpies of 88 kJ/kg in run 1.1, 60 kJ/kg in run 1.2, and 22 kJ/kg in run 1.3.

The second tested suspension medium was rapeseed oil. Discharging results, again consisting of the temperature increase over time, for the system $ZnSO_4 \cdot H_2O$ in rapeseed oil are given in 4.13 for all runs.

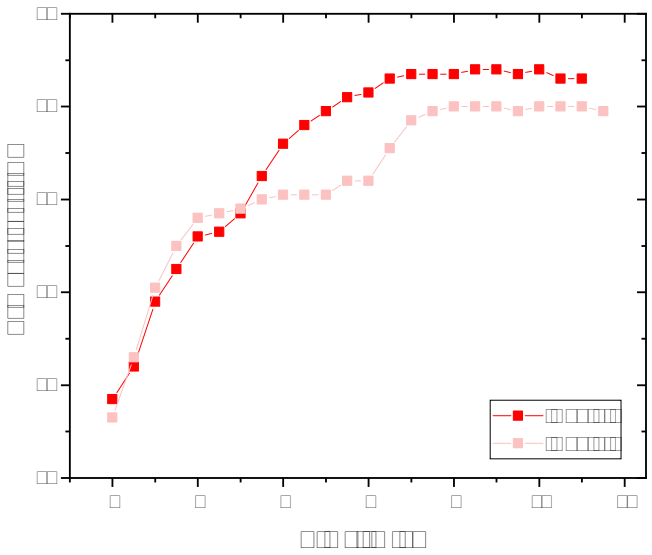

Figure 4.13: Experimental results for the discharging reaction of $ZnSO_4 \cdot H_2O$ in rapeseed oil for two runs

The temperature increased by 7.1 °C in run 1.1 and 6.7 °C in run 1.2. This corresponds to 64 kJ/kg and 57 kJ/kg. There are no results for run 1.3 as agglomeration terminated the experiment beforehand. It takes about 8 min to reach the maximum temperature.

An exemplary temperature profile for the discharging reaction of $ZnSO_4 \cdot 7\,H_2O$ in silicone oil is depicted in figure 4.14. The temperature increased only by 3 °C, which corresponds to 21 kJ/kg. These unsatisfactory results are due to agglomeration, which leads to a reduction of active reaction sides. Again, due to agglomeration, only one run was possible.

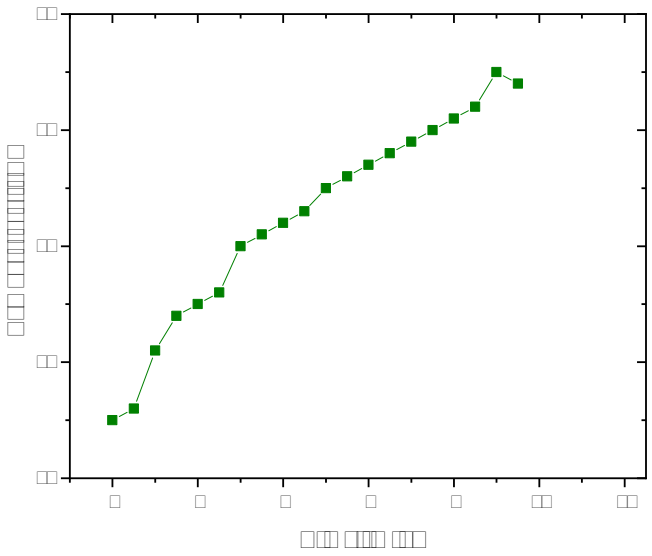

Figure 4.14: Experimental results for the discharging reaction of $ZnSO_4 \cdot H_2O$ in silicone oil

In order to compare the three different suspension mediums, exemplary plots of the discharging reaction for all suspension media are depicted in figure 4.15. In general, the addition of water to the salt $ZnSO_4 \cdot H_2O$ leads to a temperature increase over time.

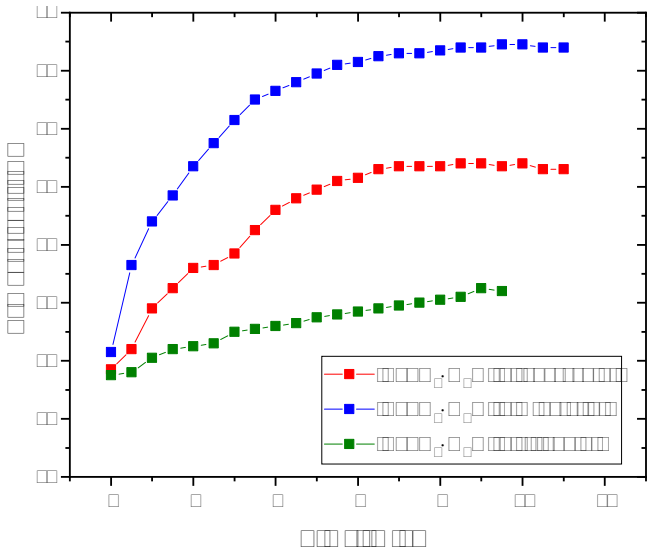

Figure 4.15: Experimental results for the discharging reaction of $ZnSO_4 \cdot H_2O$ in three different suspension media

The comparison of zinc sulphate in the different suspension media shows, that the highest temperature increase was achieved in mineral oil, with a specific energy output of 88 kJ/kg, followed by zinc sulphate in rapeseed oil. However, all values show uncertainty due to the occurrence of agglomeration. These experimental results are promising but need to be improved compared to the theoretical value of 215 kJ/kg. Apart from this, the main disadvantage is agglomeration which needs to be solved for the reliable use of the material in thermochemical energy storage applications.

4.3 Iron sulphate

Iron sulphate was tested in mineral oil for several runs. The experimental results of the charging reaction, including the conversion over time and the according temperature profile, are shown in 4.16.

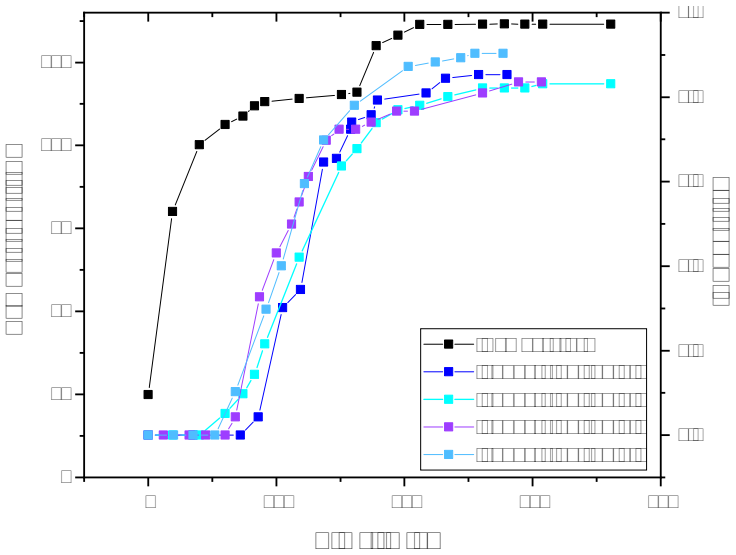

Figure 4.16: Experimental results for the charging reaction of $FeSO_4 \cdot 7\,H_2O$ in mineral oil

In this plot, two sets of each two runs of $FeSO_4 \cdot 7\,H_2O$ in mineral oil are plotted. The first two runs were carried out in the small-scale setup and the second two runs in the bigger-scale setup. As expected, no recognizable differences were found. The conversion is between 83-90% for all runs. Since only two runs were possible, no indication of changes in conversion with more runs and thus cycle stability are found. Unfortunately, agglomeration occurred, leading to a termination of the process and negatively influencing the results. The agglomeration can be explained with the low melting temperature of 64 °C of $FeSO_4 \cdot 7\,H_2O$ [6]. Dehydration started at around 100 °C and lasted for approx. 5 h in all runs.

The discharging of iron sulphate was done by adding water to the system and recording the resulting temperature change. In 4.17 the experimental results of the discharging reaction are shown.

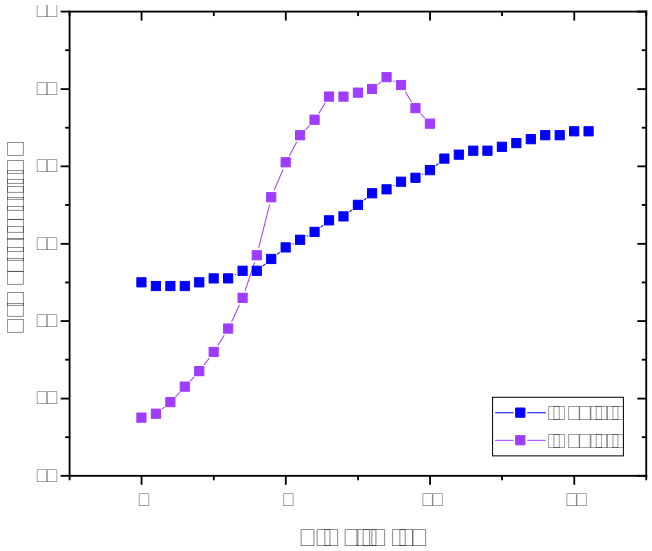

Figure 4.17: Experimental results for the discharging reaction of $FeSO_4 \cdot H_2O$ in mineral oil

Due to agglomeration, only the first run of each experiment (run 1.1 and run 2.1) could be continued with a discharging reaction. In the second charging cycle, agglomeration was severe resulting in a blockade of the stirring and thus termination of the reaction. The temperature increased by 3.9 °C in run 1.1 and 8.9 °C in run 2.1. This corresponds to 29 kJ/kg in run 1.1 and 57 kJ/kg in run 2.1. The big difference between the two runs can be explained by agglomeration. Depending on the agglomerate size, more or less reaction sides are available, resulting in a change in temperature increase. The experimental energy output is only 27% of the theoretical energy density (210 kJ/kg).

4.4 Aluminium sulphate

Charging of $Al_2(SO_4)_3 \cdot 18\,H_2O$ in mineral oil was performed in the three-neck flask setup by heating up the suspension. Conversion and temperature results are shown in figure 4.18. Three runs of aluminium sulphate in mineral oil were conducted. In the first run 1.1 a conversion of only 56% was achieved. Run 1.2 showed a conversion of 96% and run 1.3 only 75%. On the one hand, the differences in conversion can be explained because of the stoichiometric addition of water to the system and thus accumulation in the system. On the other hand, agglomeration occurred and therefore the conversion was decreased. The dehydration reaction started at 117 °C in run 1.1, although decreased in subsequent cycles.

In run 1.2 and run 1.3 the dehydration reaction starts at 115°C and 100°C, indicating that unbound water is in the system. The temperature profile of each run varies strongly, which can be explained based on the setup condition of setting the temperature profile manually for every run. Thus only little information about the duration of the charging process is available. However, run 1.1 lasted for approx. 8 h, run 1.2 for only 2 h and run 1.3 for 4 h. Unfortunately, slight agglomeration occurred in all runs, but was reversed during the discharging process. Foaming was negligible.

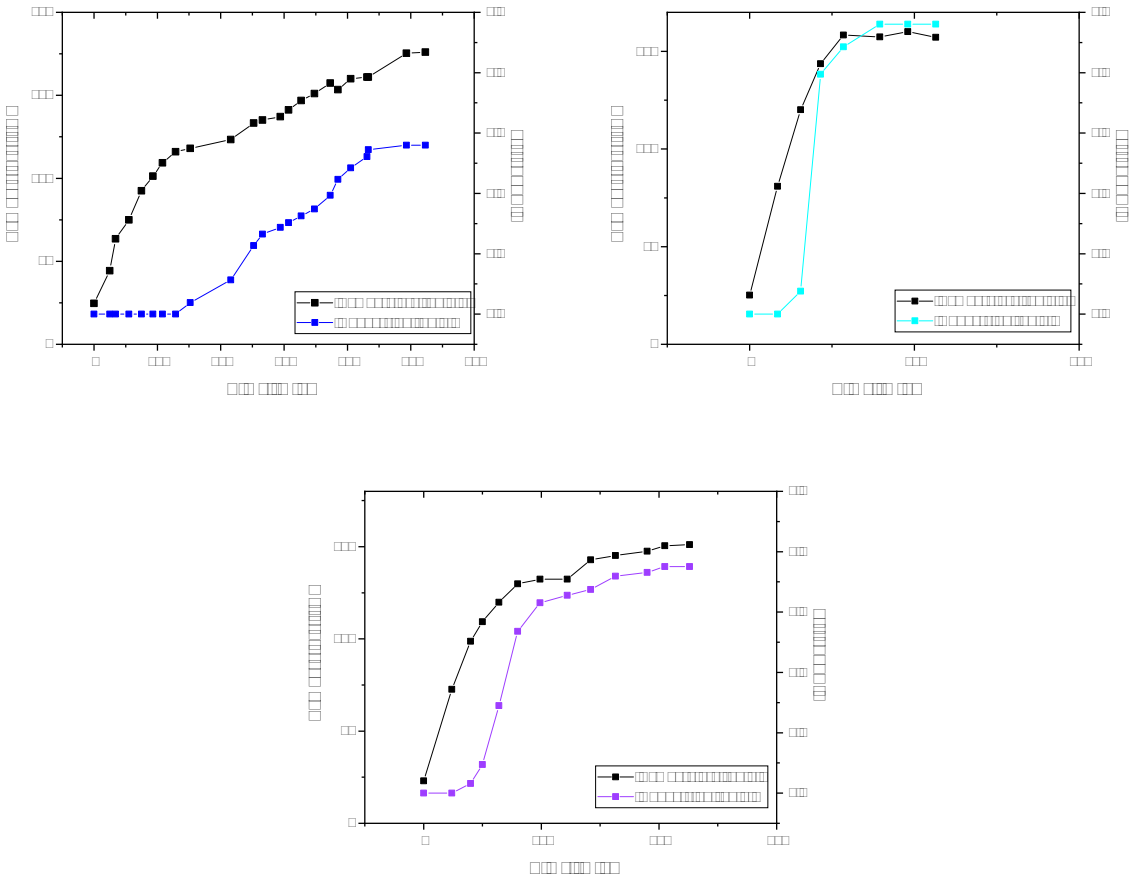

Figure 4.18: Experimental results for the charging reaction of $Al_2(SO_4)_3 \cdot 18\,H_2O$ in mineral oil for three runs

Discharging was performed after each run by adding water to the system. The change in temperature was recorded and the results of all three runs are depicted in figure 4.19. The temperature increased only slightly in all three runs. The temperature increase in the first run is only 1.2 °C, in the second run 2.2 °C, and in the third run again only 1.1 °C. This corresponds to a specific reaction enthalpy of only 19 kJ/kg in run 1.1, 24.2 kJ/kg in run 1.2, and 14.3 kJ/kg in run 1.3. Reasons for the low energy output might be the low conversion or agglomeration during the dehydration reaction of the charging process. Nevertheless, the low energy output seems to be a common problem, as stated in the literature [44]. During discharging no agglomeration occurred, instead, quite the reverse happened and the agglomerates disintegrated.

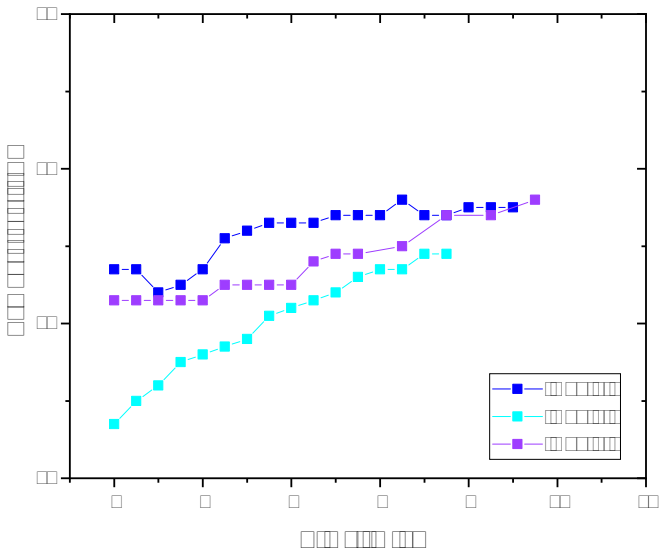

Figure 4.19: Experimental results for the discharging reaction of $Al_2(SO_4)_3 \cdot 18\,H_2O$ in mineral oil

4.5 Potassium zinc sulphate

Potassium zinc sulphate in mineral oil was tested preliminary in the three-neck flask setup. Results were promising thus, experiments were performed in the up-scaled reactor. Experimental results of the discharging reaction are shown in figure 4.20.

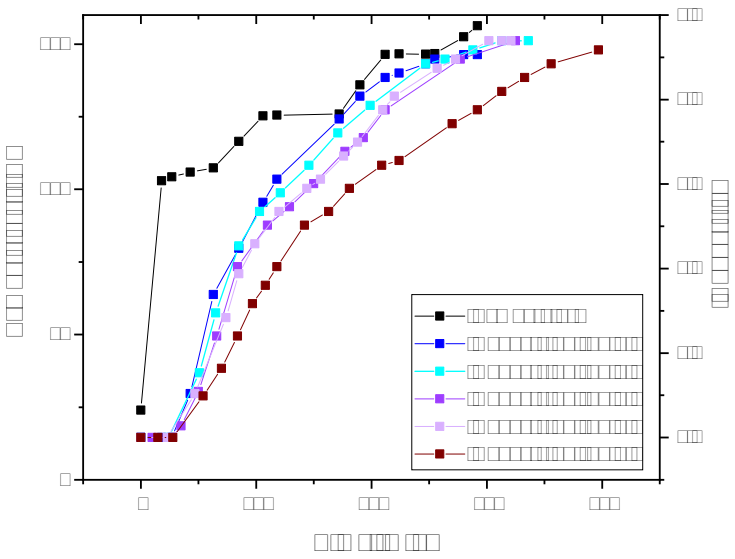

Figure 4.20: Experimental results for the charging of $K_2Zn(SO_4)_2 \cdot 6\,H_2O$ in mineral oil

The temperature profile is the same for all five runs, thus only one is depicted. The conversion of run 1.1 is 91%, slightly higher in run 1.2 with 95%, and about the same in run 1.3 with 94%. Run 1.4 has a conversion of again 94% and run 1.5 of 92%. Except for small deviations, the conversion is almost the same for all runs, thus the material seems to be stable for several cycles. Moreover, no agglomeration, but unfortunately strong foaming at the beginning of the dehydration reaction happened.

The discharging process was done by adding a stoichiometric amount of water to the system. The recorded change in temperature is plotted in figure 4.21.

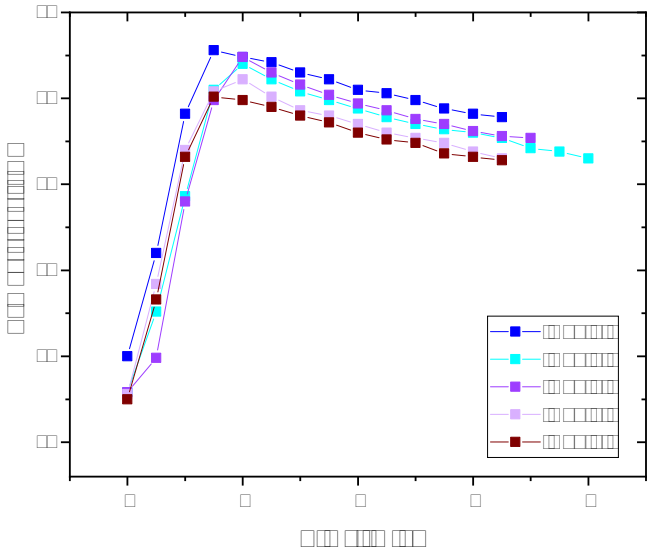

Figure 4.21: Experimental results for the discharging reaction of $K_2Zn(SO_4)_2 \cdot 6\,H_2O$ in mineral oil for five runs

The temperature increase of all five runs is similar. The maximum temperature increase of 19.5 °C was achieved in run 1.3, followed by run 1.2 with a temperature increase of 19.1 °C and run 1.4 with an increase of 18.3 °C. Run 1.1 reached a temperature increase of 17.8 °C and run 1.5 an increase of 17.6 °C. This corresponds to an energy output of 94 kJ/kg in run 1.3, 92 kJ/kg in run 1.2, 89 kJ/kg in run 1.1 as well as run 1.4 and 86 kJ/kg in run 1.5. Consequently, up to 50% of the theoretical energy density of 191 kJ/kg were achieved. It took about 2 min for all runs to reach the maximum temperature, which indicates fast kinetics of the reaction. All in all, this material is promising for TCES as a high conversion, high experimental energy density, and good cycle stability were achieved. Moreover, no agglomeration occurred.

4.6 Potassium magnesium sulphate

The whole storage process is experimentally investigated to get detailed information on important properties such as experimental energy density, conversion, and cycle stability. The results for the charging process, including conversion and temperature over time of $K_2Mg(SO_4)_2 \cdot 6\,H_2O$ in mineral oil are plotted in figure 4.22.

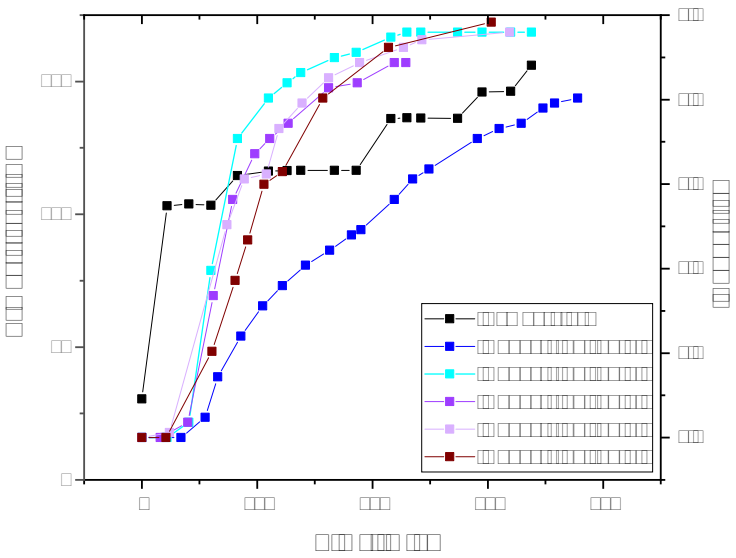

Figure 4.22: Experimental results for the charging reaction of $K_2Mg(SO_4)_2 \cdot 6\,H_2O$ in mineral oil for five runs

The conversion in run 1.1 is only 81%, but after adding the stoichiometric amount of water, the conversion in run 1.2 is higher at 96%. The conversion in run 1.3, run 1.4, and run 1.5 stays at a high level with 96%, 89%, and 98%. The conversion is similar for all runs except run 1.1. A possible explanation might be, that during the drying after synthesis in a vacuum atmosphere of 50 mbar, some of the bound water was lost and the material already dehydrated to a certain amount. Another reason might be, that the conversion of the educts to $K_2Mg(SO_4)_2 \cdot 6\,H_2O$ during synthesis was not completed and thus the yield of $K_2Mg(SO_4)_2 \cdot 6\,H_2O$ was less than 100%. Consequently, some of the educt K_2SO_4 would be left in the reactor and work as a filler, instead of contributing to the storage itself. The dehydration reaction starts at 103-104 °C and lasts about 4-6 h in all runs.

The discharging process was investigated by adding a stoichiometric amount of water to the suspension and measuring the temperature change. Those experimental results are plotted in figure 4.23. The temperature increase is about the same for all runs. Run 1.1 achieves an increase of 10.7 °C, run 1.2 showed an increase of 11.1 °C which both corresponds to 54 kJ/kg. During run 1.3 and run 1.4 the temperature increased by 10.3 °C which corresponds to 52 kJ/kg. In run 1.5 the temperature increased by 10.1 °C which

corresponds to 50 kJ/kg. It took about 4-8 min to reach maximum temperature, which indicates that kinetics are slower compared to $K_2Zn(SO_4)_2 \cdot 6\,H_2O$.

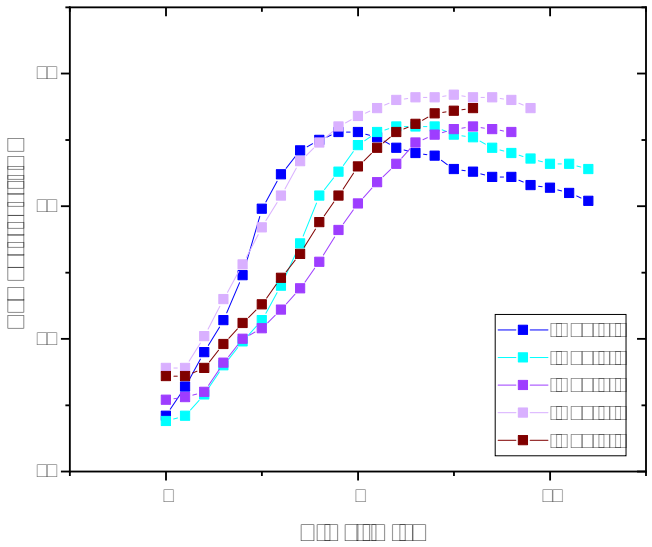

Figure 4.23: Experimental results for the discharging reaction of $K_2Mg(SO_4)_2 \cdot 6\,H_2O$ in mineral oil for five runs

4.7 Potassium copper sulphate

This Tutton salt was tested in mineral oil for five runs. During charging, the conversion and temperature profile was evaluated and the results are shown in figure 4.24. The conversion of all five runs is high with 92% in the first, 100% in the second, 90% in the third, 99% in the fourth, and 90% in the fifth run. This corresponds to 94% in average. The dehydration starts at around 105 °C in all runs. It needs to be mentioned that during the dehydration reaction heavy foaming occurred and consequently solid material stuck to the reactor lid. Thus small quantities of material were lost each run and led to falsification of the results. During the charging reaction, a colour change was observed. The starting product $K_2Cu(SO_4)_2 \cdot 6\,H_2O$ was blue and turned into the light blue product $K_2Cu(SO_4)_2$.

The discharging reaction was performed by adding stoichiometric amounts of water to the system. In figure 4.25 the resulting temperature increase is shown. The temperature increased by 13.0 °C in the first run, followed by 12.2 °C in the second run. In the third, fourth, and fifth run the temperature increased less by only 5.9 to 8.3 °C. A possible explanation for this decrease is that with each run more and more solid material was lost due to foaming. The temperature increases correspond to an energy output of 64 kJ/kg in the first run 1.1, 59 kJ/kg in the second run 1.2, and 30-56 kJ/kg in the third, fourth, and fifth run. The average value of 49 kJ/kg is only 22% of the theoretical energy density

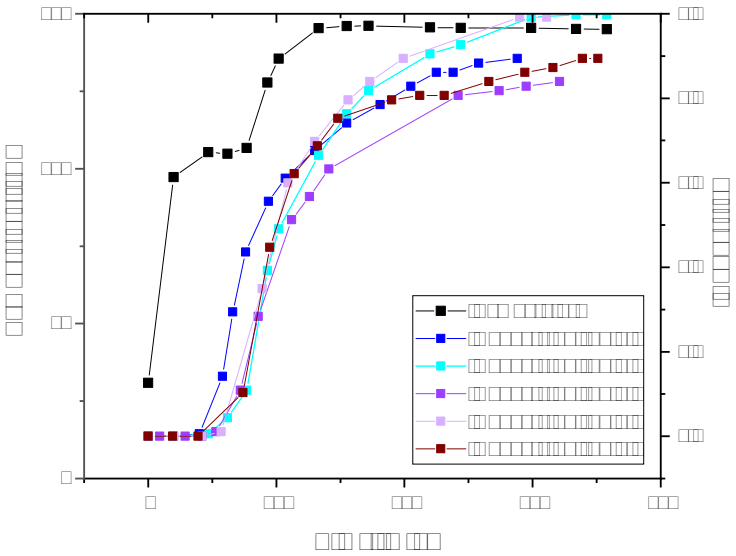

Figure 4.24: Experimental results for the charging reaction of $K_2Cu(SO_4)_2 \cdot 6\,H_2O$ in mineral oil for five runs

of 225 kJ/kg. It takes up to 5 min to reach the maximum temperature, which indicates fast reaction kinetics. Apart from this, a reverse color change from light blue to blue was observed during this reaction.

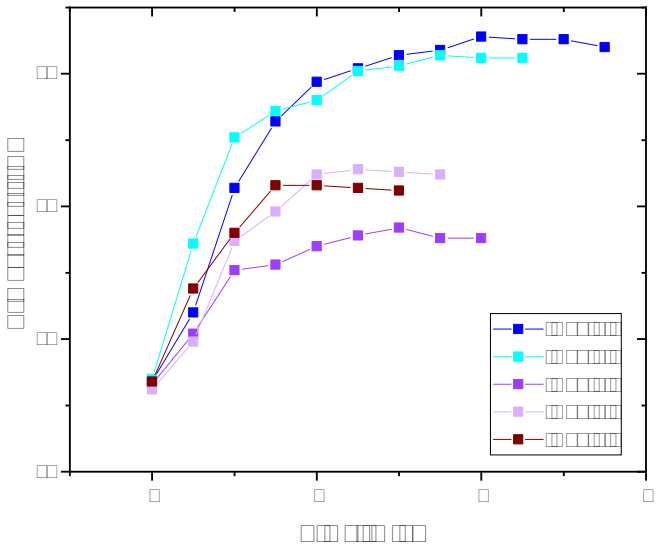

Figure 4.25: Experimental results for the discharging reaction of $K_2Cu(SO_4)_2$ in mineral oil for five runs

4.8 Strontium bromide

The experimental results of strontium bromide are discussed in this section. First, the discharging process is investigated by comparing the conversion over time and the temperature of several runs. In figure 4.26 an illustration of the results is given.

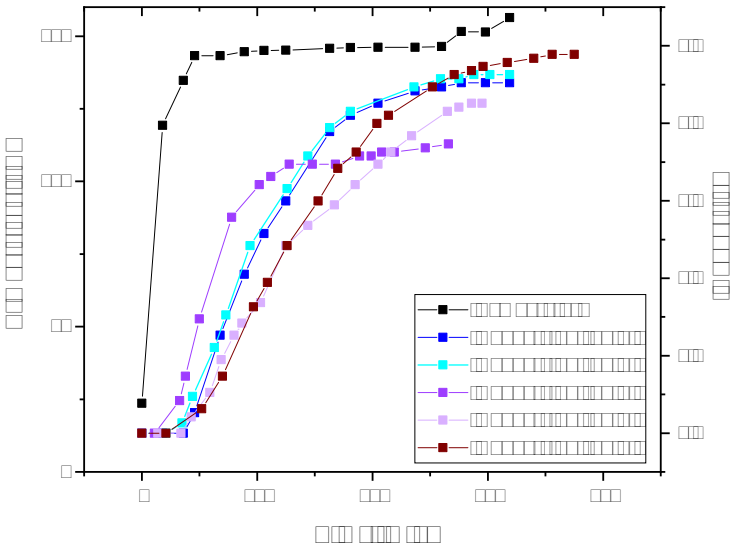

Figure 4.26: Experimental results for the charging reaction of $SrBr_2 \cdot 6\,H_2O$ in mineral oil

During the charging reaction, strontium bromide hexahydrate was dehydrated to the monohydrate. The conversion of this reaction was 91% in run 1.1, 93% in run 1.2 but only 75% in run 1.3. It increased again in run 1.4 with 87% and even more in run 1.5 with 99%. The reason for the variations in conversion might be agglomeration which occurred during the charging process of all runs. Another possible explanation is the addition of a stoichoimetric amount of water during discharging and thus accumulation of water in the system. The dehydration reaction started at 141-143 °C and lasted for about 4.5-5.5 h in all runs. At the beginning of the dehydration reaction agglomeration occurred, then the formation of small transparent crystals, which indicates a phase change. There was no foaming during the dehydration phase.

The results of the discharging process are given in figure 4.27. The highest temperature increase of 7.0 °C was achieved in run 1.1, followed by run 1.2 with 6.0 °C, run 1.3 with 5.7 °C and run 1.5 with 5.7 °C. The lowest temperature increase of 4.7 °C was achieved in run 1.4. During the reaction, agglomeration of the transparent crystals to white agglomerates took place. The specific reaction enthalpy corresponds to the temperature increase, thus the highest value of 40 kJ/kg is achieved in run 1.1, followed by run 1.2 and run 1.3 with 35 kJ/kg. Run 1.4 achieves only 29 kJ/kg and run 1.5 33 kJ/kg. It takes about 1.5 to 4 min to reach the maximum temperature, which indicates fast reaction kinetics.

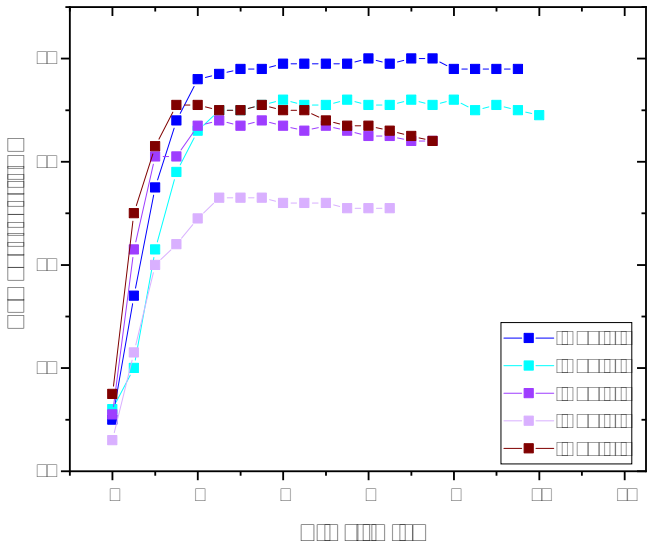

Figure 4.27: Experimental results for the discharging reaction of $SrBr_2 \cdot 6\,H_2O$ in mineral oil

4.9 Zeolite 4A

Zeolites rely on a different storage principle than all the other investigated systems. The adsorption/desorption principle is described in more detail in chapter 2.4.7. First, the discharging of zeolite 4A was investigated and the conversion and the related temperature profile over time were evaluated. The results can be seen in figure 4.28.

In run 1.1 no water was collected, even though slight foaming occurred at the beginning of the reaction. On the one hand, the zeolite was in an almost dry state. On the other hand, the reaction temperature was maybe not high enough as temperatures over 170 °C are required for the discharging reaction. After rehydration in run 1.1 with 30 wt% water, a dehydration reaction took place in run 1.2 and run 1.3. The conversion is 57% in run 1.2 and 78% in run 1.3. The dehydration reaction starts at a temperature of 100 °C which indicates that probably not all water from run 1.1 was bound. No agglomeration was visible, quite the reverse, after run 1.3 the zeolites still were beads of the same size as in the beginning. The dehydration in run 1.2 and run 1.3 lasted for 5-6 h.

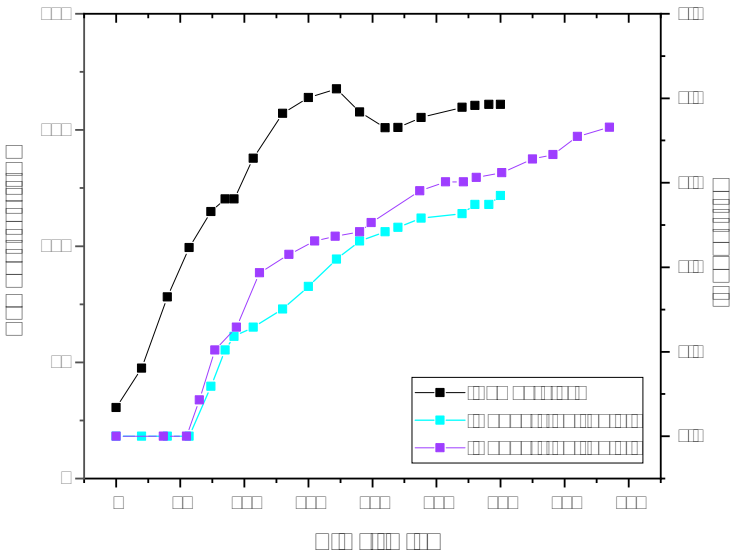

Figure 4.28: Experimental results for the charging reaction of zeolite 4A in mineral oil

Discharging was done by adding 30 wt% water of the zeolite to the suspension. The recorded temperature change can be seen in figure 4.29.

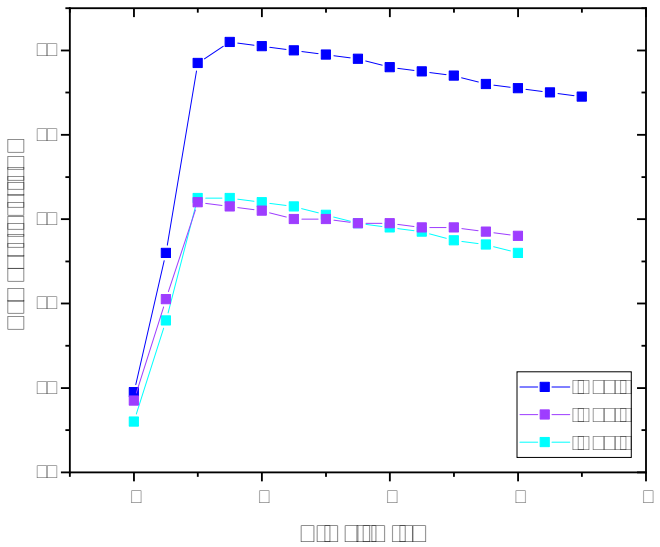

Figure 4.29: Experimental results for the discharging reaction of zeolite 4A in mineral oil

The temperature increased by 8.3 °C in run 1.1, 5.3 °C in run 1.2, and 4.7 °C in run 1.3. This corresponds to 68 kJ/kg in run 1.1, 41 kJ/kg in run 1.2, and 35 kJ/kg in run 1.3.

The low energy output in the second and third run can be explained by the low conversion during the charging phase. It only took 1-1.5 min to reach the maximum temperature, which indicates fast reaction kinetics.

4.10 Magnesium chloride

Magnesium chloride is a potential TCES material due to promising properties stated in chapter 2.4.8. The charging process was investigated and the results, including conversion and temperature over time, are depicted in figure 4.30.

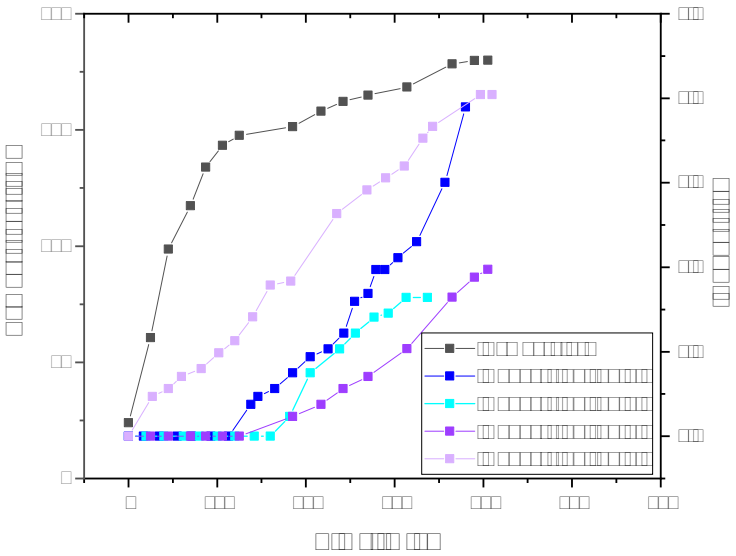

Figure 4.30: Experimental results for the charging reaction of $MgCl_2 \cdot 6\,H_2O$ in mineral oil for two sets of two runs

Two sets of two runs were carried out, but conversion differs greatly. In run 1.1 a conversion of 78% was reached, which decreased drastically in run 1.2 with only 34%. On the contrary, in run 2.1 the conversion is only 40% and increased in run 2.2 to 81%. Dehydration starts at 148-151 °C in all runs except run 1.2 with a dehydration temperature of 172 °C. The reason for this deviation might be measurement inaccuracy, as the temperature and conversion is measured discontinuously. Unfortunately, during the charging reaction, a phase change from solid to liquid occurred at around 127 °C. The liquid phase is not miscible with the mineral oil. During the cooling phase, the liquid phase solidifies in one big chunk.

The discharging was performed by adding water to the system and measuring the temperature increase. In figure 4.31 the results are shown.

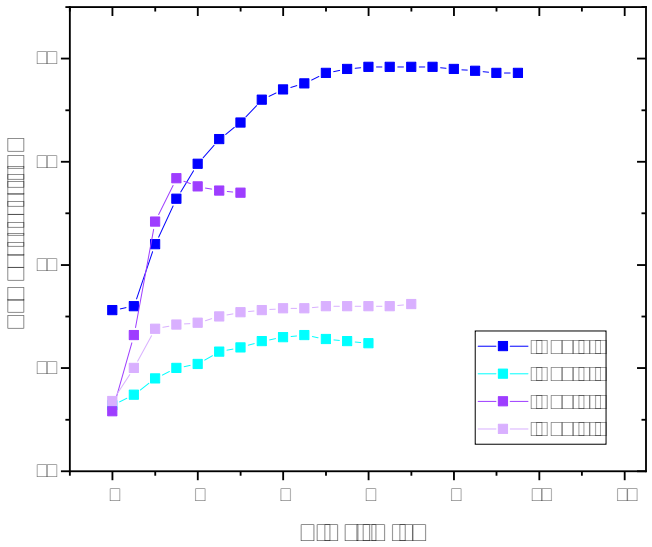

Figure 4.31: Experimental results for the discharging reaction of $MgCl_2 \cdot 6\,H_2O$ in mineral oil for two sets of two runs

Due to the solidification of the liquid phase in a big chunk after the charging reaction, discharging reaction is difficult to perform as stirring is not possible anymore. Nevertheless, the temperature increased by 11.7 °C in run 1.1 and 11.3 °C in run 2.1, which corresponds to 115 kJ/kg and 98 kJ/kg. The temperature change decreased massively in run 1.2 with 3.8 °C and run 2.1 with 4.7 °C, which corresponds to 31 kJ/kg and 39 kJ/kg. The reason for the decreased temperature change is the solidification in one big chunk after the phase change and thus the limited availability of reaction sites. The rehydration reaction needed up to 7 min to reach the maximum temperature, which also results from the formed solid.

4.11 Strontium chloride

Strontium chloride was charged by dehydrating the hexahydrate to the monohydrate. The conversion of this reaction over time and the according temperature profile are examined and the results depicted in figure 4.32. Three individual results of $SrCl_2 \cdot 6\,H_2O$ in mineral oil were carried out. Several runs in a row were not possible, as a phase change from solid to liquid occurred during the heating of the material and subsequent solidification. The dehydration reaction started at around 120 °C and reached a conversion of 80% in all runs. The dehydration reaction lasted for about 6-7 h.

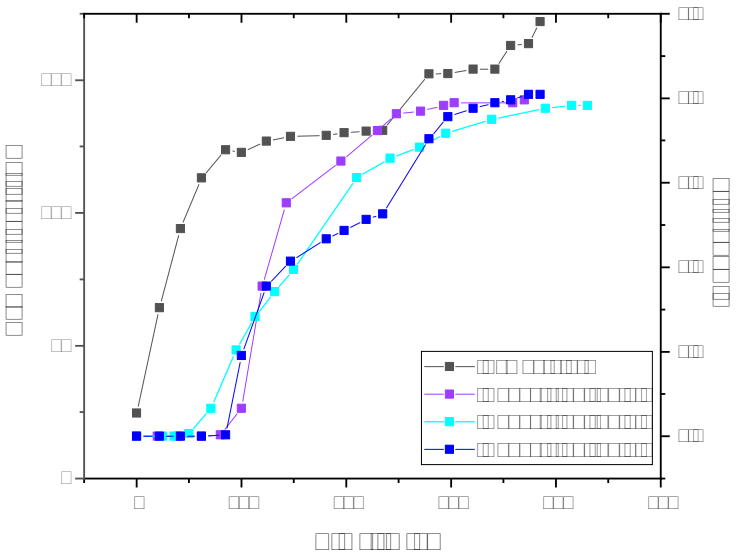

Figure 4.32: Experimental results for the charging reaction of $SrCl_2 \cdot 6\,H_2O$ in mineral oil for three runs

Discharging results of strontium chloride in mineral oil are given in figure 4.33. The differences in temperature increase between the individual runs are shown.

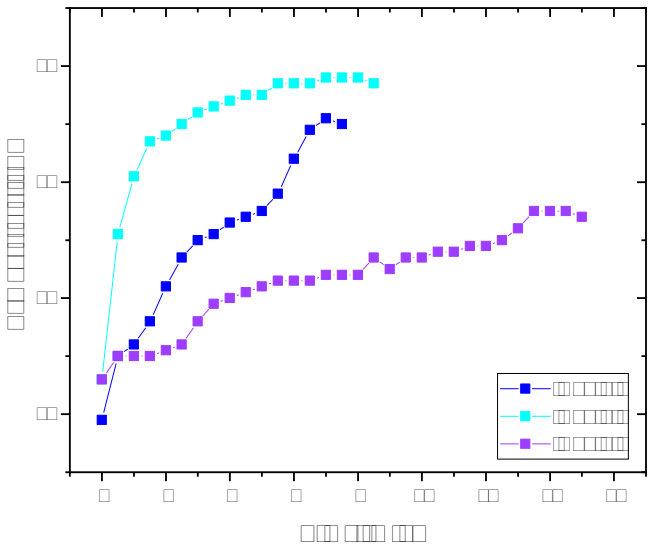

Figure 4.33: Experimental results for the discharging reaction of $SrCl_2 \cdot 6\,H_2O$ in mineral oil for three runs

The temperature increased by 5.2 °C in the first two runs, which corresponds to 28 kJ/kg in run 1.1 and 30 kJ/kg in run 2.1. In run 3.1 the temperature increased by 2.9 °C which correlates to 17 kJ/kg. It took 7 min in the first two runs to reach the maximum, but 15 min in the third run. All the deviations in the third run can be explained by differences in the uncontrollable solidification during the cooling phase.

4.12 Potassium oxalate

Potassium oxalate in mineral oil was tested in the small-scale three-neck flask setup to get a first impression of the behavior of the material for TCES applications. In figure 4.34 the experimental results of the charging reaction, consisting of conversion and temperature over time, are shown.

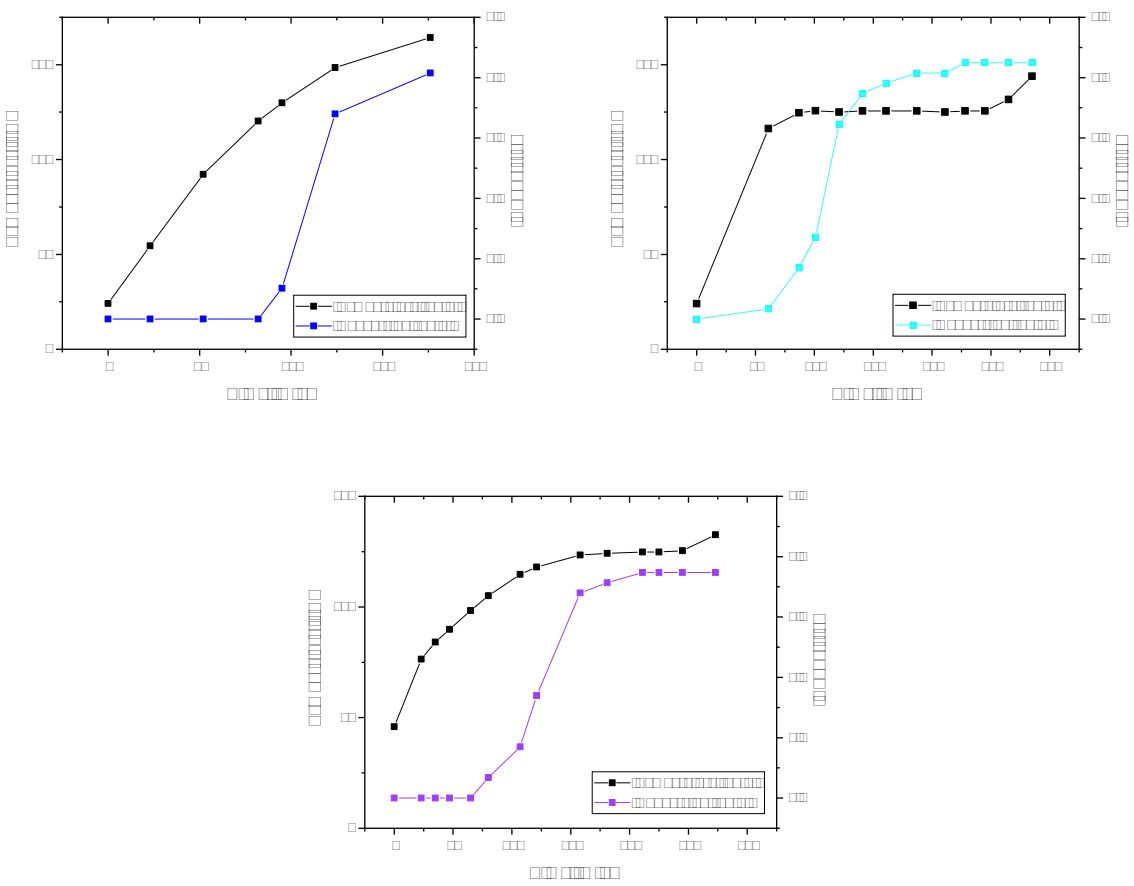

Figure 4.34: Experimental results for the charging reaction of $K_2C_2O_4 \cdot H_2O$ in mineral oil for three runs

In general, the conversion is high in all three runs, even though three different temperature profiles have been applied. In run 1.1 and run 1.3 the conversion is 83%, in run 1.2 it is 86%. The theoretical amount of condensed water is low, therefore, small deviations

have a great impact. The reaction started at 129 °C in run 1.1, 116 °C in run 1.2, and already at 105 °C in the third run. This indicates that unbound water accumulated in the system. The dehydration reaction lasted for 3-4 h, depending on the temperature profile. No agglomeration or foaming happened during the dehydration reaction.

The discharging of $K_2C_2O_4 \cdot H_2O$ was evaluated by measuring the temperature change after the addition of stoichiometric amounts of water. The experimental results can be found in figure 4.35.

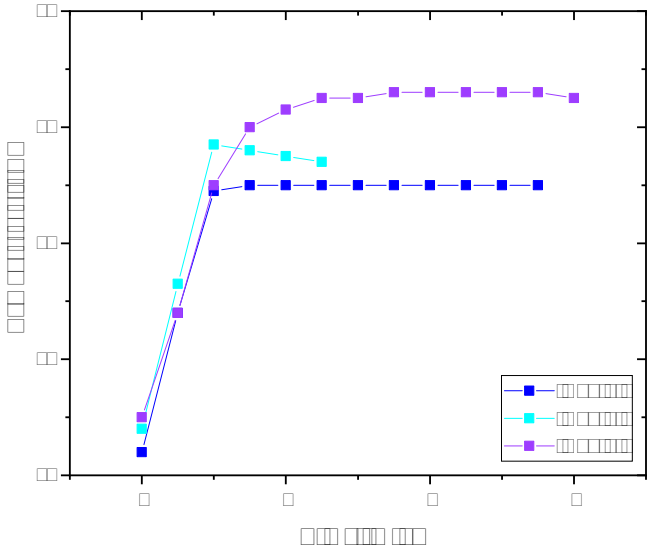

Figure 4.35: Experimental results for the discharging reaction of $K_2C_2O_4 \cdot H_2O$ in mineral oil

The temperature increased by 4.6 °C in run 1.1, 4.9 °C in run 1.2, and 5.6 °C in run 1.3. Which corresponds to 29 kJ/kg in the first run, 31 kJ/kg in the second run, and 36 kJ/kg in the third run. The temperature increase and thus energy output is low for all runs. This results from the low theoretical energy density of only 70 kJ/kg. The rehydration reaction was fast, it only took 1-3 min to reach the maximum temperature.

4.13 Calcium sulphate

Calcium sulphate dihydrate was tested as a possible TCES material in the three-neck flask setup. During charging the dihydrate reacts to the anhydrous salt theoretically. The experimental results, consisting of conversion and temperature over time, are shown in figure 4.36.

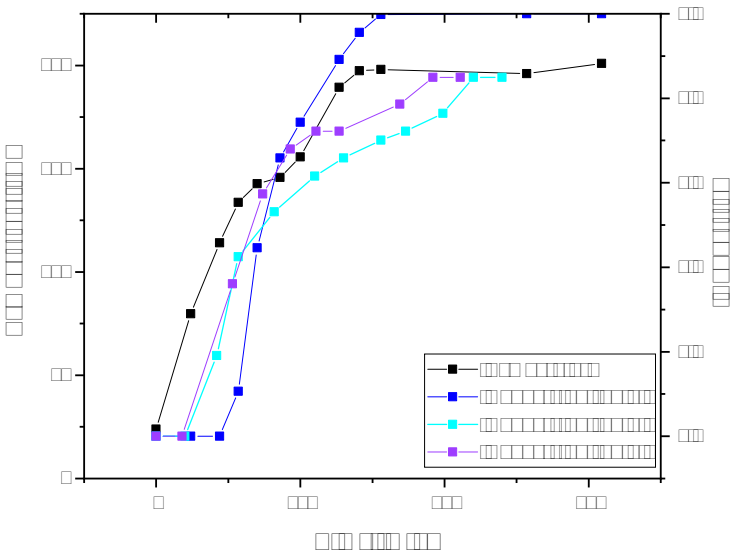

Figure 4.36: Experimental results for the charging reaction of $CaSO_4 \cdot 2\,H_2O$ in mineral oil

Three runs of $CaSO_4 \cdot 2\,H_2O$ in mineral oil were tested. In the first run, a 100% conversion was reached, which decreased in the second and third run to 85%. The decrease in the results indicates poor reversibility of the reaction in real conditions. In literature the formation of a stable, less reactive anhydrous phase at 250 °C was reported, supporting the assumptions above [51]. Consequently, the applied reaction conditions must be carefully set to ensure reversibility of the reaction. The dehydration reaction started at 133 °C in the first run, but already at around 105 °C in the second and third run, which indicates unbound water in the system. This also supports the assumption regarding the formation of a less reactive anhydrous phase. The reaction lasted for 5 h in the first run, which also decreased for the second and third run with about 3.5 h. A possible reason for that is again unbound water in the system, which evaporated more easily. It needs to be mentioned, that foaming happened during the charging process, but fortunately, no agglomeration was observable.

The discharging of the charged calcium sulphate was done by adding a stoichiometric amount of water to the system. The resulting temperature increase was recorded and is shown in figure 4.37. The temperature increased by 6.4 °C in the first run, 5.5 °C in the second run and only 4.0 °C in the third run. This corresponds to a energy output of 46 kJ/kg in the first run, 40 kJ/kg in the second run and 30 kJ/kg in the third run. These results also support the assumptions about the formation of a less reactive phase during the charging reaction. The energy output is low but reaches up to 60% of the theoretical energy output of 78 kJ/kg with liquid water. It takes about 3-4.5 min to reach the maximum temperature, which indicates relatively fast reaction kinetics.

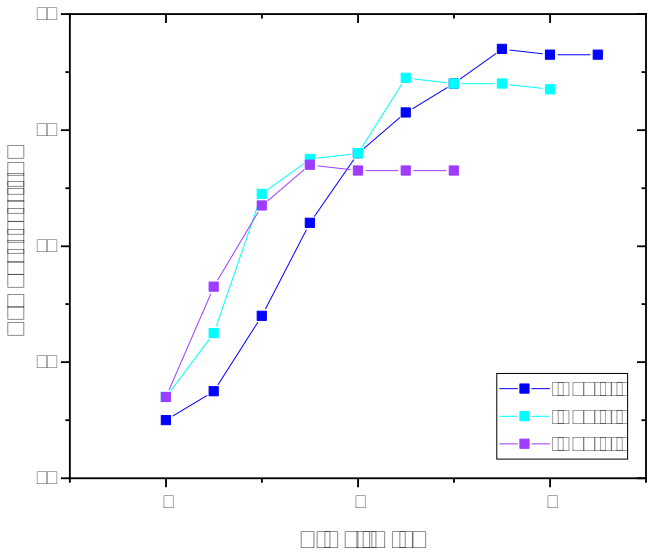

Figure 4.37: Experimental results for the discharging reaction of $CaSO_4 \cdot 2\,H_2O$ in mineral oil

4.14 Magnesium bromide

Magnesium bromide hexahydrate was dehydrated during the charging process. The conversion of this reaction and the according temperature profile are plotted for several runs in figure 4.38. Two experiments with three runs in total were performed. More runs were not possible, due to phase change phenomena during the charging process, as subsequent solidification of the liquid phase into a big solid during the storage period leads to a blockage of the stirring. The conversion in run 1.1 is only 26%. The conversion in run 2.1 is again low at 46%, but high in run 2.2 at 95%. A possible reason for the low conversion in both first runs is the phase change from solid to liquid at around 160-170 °C. This corresponds to the melting temperature of $MgBr_2 \cdot 6\,H_2O$ of 165 °C [58]. The high conversion in the second run can be explained by the stoichiometric addition of water during the discharging reaction and thus accumulation of water in the system. The dehydration starts at around 150 °C in all three runs. This indicates that probably only the first reaction step to the tetrahydrate $MgBr_2 \cdot 4\,H_2O$ in (2.54) is reached, which can also be seen in the low conversion. Consequently, a possible solution might be to increase the applied temperature above 200 °C to reach a higher conversion, which is not possible with the current setup.

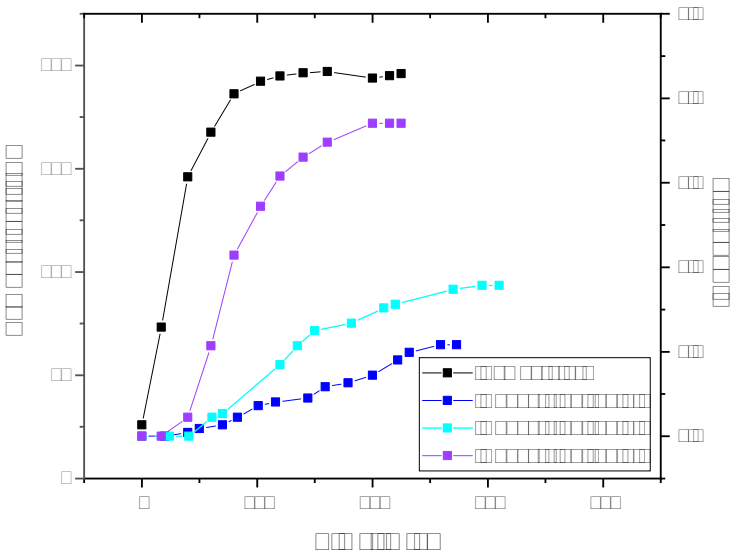

Figure 4.38: Experimental results for the charging reaction of $MgBr_2 \cdot 6\,H_2O$ in mineral oil

During the discharging the reverse reaction takes place and heat is released, leading to a temperature increase. In figure 4.39 the experimental results of this reaction are shown and the differences between the individual runs evaluated.

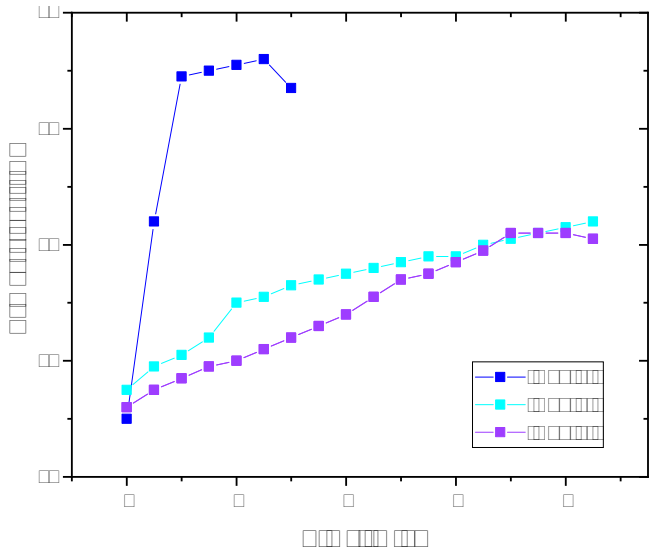

Figure 4.39: Experimental results for the discharging reaction of $MgBr_2 \cdot 6\,H_2O$ in mineral oil

The temperature increased by 6.2 °C in the first run, but only by 3 °C in the second and third run. This corresponds to 47 kJ/kg in the first run, 24 kJ/kg in the second, and 22 kJ/kg in the third run. This is low compared to the theoretical energy density of 108 kJ/kg with liquid water. This results from the phase change during the charging process and the subsequent solidification of the liquid in one big solid. Consequently, the available reaction sides are massively reduced and moreover stirring is not possible anymore. This might also be the reason why it takes up to 9 min to reach the maximum temperature.

4.15 Manganese sulphate

$MnSO_4 \cdot 4\,H_2O$ was tested in mineral oil starting with the charging process to dehydrate the salt to the monohydrate $MnSO_4 \cdot H_2O$. The system was heated to the maximum of 200 °C, but no reaction took place and thus no water was evaporated. Theoretically, the reaction should start below 170 °C, but it seems that the applied temperature was not enough. Consequently, this material is not suitable for TCES in the required temperature range and thus is not further investigated.

5 Conclusion

In this chapter, the experimental results of all tested systems are summarized and compared. The average conversion X_i, the average dehydration temperature at the reaction start T_{dehyd}, the average maximal temperature at the reaction end $T_{dehyd,max}$ and the average reaction time t_R during the charging process are given. Additionally the average temperature increase, the average experimental energy output $\Delta h_{m,exp.}$ and the theoretical energy output $\Delta h_{m,theo.}$ as well as a comparison of these values $\frac{\Delta h_{m,exp.}}{\Delta h_{m,theo.}}$ are given in table 5.1. General properties of each materials system are also stated.

The highest conversion during the charging process was achieved with $K_2Cu(SO_4)_2 \cdot 6\,H_2O$, which reached a conversion of 94%, followed by the other Tutton's salts $K_2Zn(SO_4)_2 \cdot 6\,H_2O$ and $K_2Mg(SO_4)_2 \cdot 6\,H_2O$ with 93% and 92%. The lowest conversion of 56% was reached by $MgBr_2 \cdot 6\,H_2O$ followed by $MgCl_2 \cdot 6\,H_2O$ with 58%. An exception is $MnSO_4 \cdot 4\,H_2O$ which did not react at all. The remaining materials react below 200 °C and thus fulfill the required temperature range.

Unfortunately, most of the materials showed unwanted behaviour during the charging process. $MgSO_4 \cdot 7\,H_2O$, $ZnSO_4 \cdot 7\,H_2O$, $FeSO_4 \cdot 7\,H_2O$ and $Al_2(SO_4)_3 \cdot 18\,H_2O$ agglomerated which led to the termination of the reaction after several runs. $MgBr_2 \cdot 6\,H_2O$, $MgCl_2 \cdot 6\,H_2O$ and $SrCl_2 \cdot 6\,H_2O$ went through a phase change from solid to liquid and subsequently to solidification in a big block during the cooling phase. All three Tutton's salts did not agglomerate or change the phase, but foamed during the dehydration reaction, which needs to be considered when up-scaling. Zeolite A, $CaSO_4 \cdot 2\,H_2O$ and $K_2C_2O_4 \cdot H_2O$ did not show any agglomeration, phase change or foaming. However, the energy output is low.

The energy output in general is lower than theoretically expected. The reasons might be heat losses due to the experimental setup. The highest energy output with 90 kJ/kg and temperature increase of 18.5 °C was achieved by the Tutton's salt $K_2Zn(SO_4)_2 \cdot 6\,H_2O$. It is followed by $MgCl_2 \cdot 6\,H_2O$ with a significantly lower energy output of 71 kJ/kg and a temperature increase of 7.9 °C. The third highest energy output of 62 kJ/kg is achieved with $MgSO_4 \cdot 7\,H_2O$. However, as already mentioned, $MgCl_2 \cdot 6\,H_2O$ and $MgSO_4 \cdot 7\,H_2O$ are not suitable for TCES storage application as they liquefy and thus agglomerate during the cooling down phase in the case of $MgCl_2 \cdot 6\,H_2O$ or during the charging process in the case of $MgSO_4 \cdot 7\,H_2O$. However, considering agglomeration and phase changes, only six materials are usable. This are the three Tutton's salts as well as $CaSO_4 \cdot 2\,H_2O$, $K_2C_2O_4 \cdot H_2O$ and zeolite. Unfortunately, the last three mentioned substances $CaSO_4 \cdot 2\,H_2O$, $K_2C_2O_4 \cdot H_2O$ and zeolite belong to the materials with the lowest energy output of only 31-48 kJ/kg. Also $K_2Mg(SO_4)_2 \cdot 6\,H_2O$ and $K_2Cu(SO_4)_2 \cdot 6\,H_2O$ only reach a energy output of 52 kJ/kg and 48 kJ/kg. All in all, the best overall results re-

garding charging as well as discharging are achieved by the Tutton's salt $K_2Zn(SO_4)_2 \cdot 6\,H_2O$. Agglomeration is a big problem, which needs to be solved in order to use the other, commercially available substances such as $MgSO_4 \cdot 7\,H_2O$. Theoretically, this substance is very promising, but agglomeration prevents its use for TCES applications.

Table 5.1: Comparison of the average experimental results considering all runs during the charging and discharging process of each materials [46, 64]

Substance	T_{dehyd}	$T_{dehyd,max}$	X_i	t_R	ΔT	$\Delta h_{m,exp.}$[1]	$\Delta h_{m,theo.}$	$\frac{\Delta h_{m,exp.}}{\Delta h_{m,theo.}}$	**Challenges**
	$^{\circ}C$	$^{\circ}C$	%	min	$^{\circ}C$	kJ/kg	kJ/kg	%	
$MgSO_4 \cdot 7\,H_2O$	105	141	86	170	10.3	62	260	24	Agglomeration
$ZnSO_4 \cdot 7\,H_2O$	105	143	76	290	8	57	215	27	Agglomeration
$FeSO_4 \cdot 7\,H_2O$	101	140	86	100	6.3	43	210	20	Agglomeration
$Al_2(SO_4)_3 \cdot 18\,H_2O$	110	161	76	200	1.5	19	80	24	Agglomeration
$K_2Zn(SO_4)_2 \cdot 6\,H_2O$	107	148	93	340	18.5	90	191	47	Foaming
$K_2Mg(SO_4)_2 \cdot 6\,H_2O$	103	156	92	310	10.5	52	190	27	Foaming
$K_2Cu(SO_4)_2 \cdot 6\,H_2O$	105	146	94	325	9.4	49	225	22	Foaming
$SrBr_2 \cdot 6\,H_2O$	142	156	88	315	5.8	34	195	17	Agglomeration
Zeolite 4A	106	166	68	110	6.1	48	-	-	-
$MgCl_2 \cdot 6\,H_2O$	157[2]	183	58	410	7.9	71	374	19	Phase change
$SrCl_2 \cdot 6\,H_2O$	116	160	80	395	4.4	25	220	11	Phase change
$K_2C_2O_4 \cdot H_2O$	117	147	84	205	5	32	70	46	-
$CaSO_4 \cdot 2\,H_2O$	114	184	91	240	5.3	39	78	50	-
$MgBr_2 \cdot 6\,H_2O$	151	198	56	260	4.1	31	584	5	Phase change
$MnSO_4 \cdot 4\,H_2O$	>200	-	-	-	-	-	108	-	No reaction

[1] losses not taken into account
[2] outliers not considered

6 Outlook

Thermal energy storage bears great potential due to the availability of waste heat from industrial processes. Especially, thermochemical energy storage offers the possibility for efficient, long-term energy storage. The majority of waste heat is produced in the lower temperature range, thus was the focus of this work. Suitable material systems need to be investigated and therefore a systematic screening for reversible gas-solid reactions usable for thermochemical energy storage applications in a suspension reactor was performed. Some materials showed promising results, but further research is necessary. The focus of ongoing research needs to be on agglomeration behavior and prevention to get reliable storage systems. Another important parameter, which needs to be investigated more closely, is the cycle stability to ensure long usage periods. Scale-up experiments are the next logical step when a reliable system is chosen. Especially foaming needs to be considered, as it might lead to challenges in the up-scaled setup.

Bibliography

[1] Agora Energiewende. *Power Generation and Consumption*. URL: https://www.agora-energiewende.de/service/agorameter/chart/power_generation/09.01.2022/09.01.2023/today/ (visited on 01/09/2023).

[2] Salih Cem Akcaoglu et al. "Investigation of novel composite materials for thermochemical heat storage systems". In: *Energies* 13.5 (2020). ISSN: 19961073. DOI: 10.3390/en13051042.

[3] Melian A.R. Blijlevens et al. "A study of the hydration and dehydration transitions of SrCl2 hydrates for use in heat storage". In: *Solar Energy Materials and Solar Cells* 242 (2022). ISSN: 09270248. DOI: 10.1016/j.solmat.2022.111770.

[4] F Böckler et al. *Römpp Zinksulfat*. Ed. by Benjamin Oelkers. Stuttgart, Germany: Georg Thieme Verlag, 2022.

[5] Luisa F. Cabeza et al. "Introduction to thermal energy storage systems". In: *Advances in Thermal Energy Storage Systems: Methods and Applications*. Elsevier, 2020, pp. 1–33. ISBN: 9780128198858. DOI: 10.1016/B978-0-12-819885-8.00001-2.

[6] ChemicalBook Inc. *Iron sulphate heptahydrate*. URL: https://www.chemicalbook.com/ChemicalProductProperty_EN_CB9232125.htm (visited on 03/08/2023).

[7] Gülbanu Koyundereli Çılgı & Halil Cetişli. "Thermal decomposition kinetics of aluminum sulfate hydrate". In: *Journal of Thermal Analysis and Calorimetry* 98.3 (2009), pp. 855–861. ISSN: 13886150. DOI: 10.1007/s10973-009-0389-5.

[8] Tessema Derbe, Shewaye Temesgen & Mamaru Bitew. "A Short Review on Synthesis, Characterization, and Applications of Zeolites". In: *Advances in Materials Science and Engineering* 2021 (2021), pp. 1–17. ISSN: 16878442. DOI: 10.1155/2021/6637898.

[9] Markus Deutsch. "A systematic approach to identify new thermochemical energy storage systems". PhD thesis. Vienna, Austria: Technical University of Vienna, 2017.

[10] Robert E. Dinnebier, Tomče Runčevski & Kunihisa Sugimoto. "Dehydration of magnesium bromide hexahydrate studied by in situ X-ray powder diffraction". In: *Zeitschrift fur Anorganische und Allgemeine Chemie* 639.1 (2013), pp. 59–64. ISSN: 00442313. DOI: 10.1002/zaac.201200445.

[11] European Chemicals Agency. *ECHA*. URL: https://echa.europa.eu/de/information-on-chemicals (visited on 02/03/2023).

[12] Changling Feng et al. "Key technology and application analysis of zeolite adsorption for energy storage and heat-mass transfer process: A review". In: *Renewable and Sustainable Energy Reviews* 144 (2021). ISSN: 18790690. DOI: 10.1016/j.rser.2021.110954.

[13] Anton Firth, Bo Zhang & Aidong Yang. "Quantification of global waste heat and its environmental effects". In: *Applied Energy* 235 (2019), pp. 1314–1334. ISSN: 03062619. DOI: 10.1016/j.apenergy.2018.10.102.

[14] David Gilles et al. "Affordable Process for the Production of Strontium Bromide Used in Low Grade Heat Recovery Applications". In: *Procedia CIRP*. Vol. 69. Elsevier B.V., 2018, pp. 383–388. DOI: 10.1016/j.procir.2017.11.056.

[15] Global Change Data Lab. *Global direct primary energy consumption*. URL: https://ourworldindata.org/grapher/global-primary-energy (visited on 02/13/2023).

[16] V. M. Gurevich et al. "Heat capacity and thermodynamic functions of epsomite MgSO4 · 7 H2O at 0-303 K". In: *Geochemistry International* 45.2 (2007), pp. 206–209. ISSN: 00167029. DOI: 10.1134/S0016702907020103.

[17] Otto Helmboldt et al. "Aluminum Compounds, Inorganic". In: *Ullmann's Encyclopedia of Industrial Chemistry*. Vol. 2. Weinheim, Germany: Wiley-VCH Verlag GmbH & Co. KGaA, 2012, pp. 569–584. DOI: 10.1002/14356007.a01{_}527.pub2.

[18] Qiongzhu Huang et al. "Thermal decomposition mechanisms of MgCl2· 6H2O and MgCl2·H2O". In: *Journal of Analytical and Applied Pyrolysis* 91.1 (2011), pp. 159–164. ISSN: 01652370. DOI: 10.1016/j.jaap.2011.02.005.

[19] Aspen Technology Inc. *Aspen Properties*. 2023.

[20] International Renewable Energy Agency. *Renewable energy highlights Renewable electricity generation by energy source*. Tech. rep. 2022.

[21] Shun Iwasaki & Nobuyoshi Koga. "Thermal dehydration of calcium sulfate dihydrate: Physico-geometrical kinetic modeling and the influence of self-generated water vapor". In: *Physical Chemistry Chemical Physics* 22.39 (2020), pp. 22436–22450. ISSN: 14639076. DOI: 10.1039/d0cp04195e.

[22] Ndue Kanari et al. "Thermal behavior of hydrated iron sulfate in various atmospheres". In: *Metals* 8.12 (2018). ISSN: 20754701. DOI: 10.3390/met8121084.

[23] Ralf Kuder & Markus Blesl. "Technology orientated analysis of emission reduction potentials in the industrial sector in the EU-27". In: *International Energy Workshop (IEW), Stockholm, Sweden*. 2010.

[24] Ae Ran Lim & Sun Ha Kim. "Structural and thermodynamic properties of Tutton salt K2Zn(SO4)2·6H2O". In: *Journal of Thermal Analysis and Calorimetry* 123.1 (2016), pp. 371–376. ISSN: 15882926. DOI: 10.1007/s10973-015-4865-9.

[25] Jianquan Lin et al. "Applications of low-temperature thermochemical energy storage systems for salt hydrates based on material classification: A review". In: *Solar Energy* 214 (2021), pp. 149–178. ISSN: 0038092X. DOI: 10.1016/j.solener.2020.11.055.

[26] Paul MacMillan et al. "Strontium and strontium compounds". In: *Ullmann's Encyclopedia of Industrial Chemistry*. Vol. 34. 77. Weinheim, 2012, pp. 473–480. DOI: 10.1002/14356007.a25{_}321.

[27] Yoshio Masuda. "The thermal transition of anhydrous potassium oxalate". In: *Thermochimica Acta* 131 (1988), pp. 291–296.

[28] Merck KGaA. *Sigma-Aldrich Magnesium sulphate heptahydrate*. URL: https://www.sigmaaldrich.com/AT/de/substance/magnesiumsulfateheptahydrate2464710034998 (visited on 02/03/2023).

[29] Merck KGaA, Darmstadt, Germany. *Sigma-Aldrich Aluminium sulphate octadecahydrate*. URL: https://www.sigmaaldrich.com/AT/de/product/sigald/227617 (visited on 02/03/2023).

[30] Merck KGaA, Darmstadt, Germany. *Sigma-Aldrich Calcium sulphate dihydrate*. URL: https://www.sigmaaldrich.com/AT/de/substance/calciumsulfatedihydrate1721710101414 (visited on 02/03/2023).

[31] Merck KGaA, Darmstadt, Germany. *Sigma-Aldrich Copper sulphate pentahydrate*. URL: https://www.sigmaaldrich.com/AT/de/substance/copperiisulfatepentahydrate249697758998 (visited on 02/03/2023).

[32] Merck KGaA, Darmstadt, Germany. *Sigma-Aldrich Iron sulphate heptahydrate*. URL: https://www.sigmaaldrich.com/AT/de/substance/ironiisulfateheptahydrate278017782630 (visited on 02/03/2023).

[33] Merck KGaA, Darmstadt, Germany. *Sigma-Aldrich Magnesium bromide hexahydrate*. URL: https://www.sigmaaldrich.com/AT/de/product/aldrich/216844 (visited on 02/03/2023).

[34] Merck KGaA, Darmstadt, Germany. *Sigma-Aldrich Magnesium chloride hexahydrate*. URL: https://www.sigmaaldrich.com/AT/de/product/mm/105833 (visited on 02/03/2023).

[35] Merck KGaA, Darmstadt, Germany. *Sigma-Aldrich Potassium oxalate monohydrate*. URL: https://www.sigmaaldrich.com/AT/de/substance/potassiumoxalatemonohydrate184236487485 (visited on 02/03/2023).

[36] Merck KGaA, Darmstadt, Germany. *Sigma-Aldrich Potassium sulphate*. URL: https://www.sigmaaldrich.com/AT/de/substance/potassiumsulfate174267778805 (visited on 02/03/2023).

[37] Merck KGaA, Darmstadt, Germany. *Sigma-Aldrich Strontium chloride hexahydrate*. URL: https://www.sigmaaldrich.com/AT/de/substance/strontiumchloridehexahydrate2666210025704 (visited on 02/03/2023).

[38] Merck KGaA, Darmstadt, Germany. *Sigma-Aldrich Zeolite*. URL: https://www.sigmaaldrich.com/AT/de/substance/molecularsieves41234570955010 (visited on 02/03/2023).

[39] Merck KGaA, Darmstadt, Germany. *Sigma-Aldrich Zinc sulphate heptahydrate*. URL: https://www.sigmaaldrich.com/AT/de/substance/zincsulfateheptahydrate287567446200 (visited on 02/03/2023).

[40] Barbara Mette et al. "New highly efficient regeneration process for thermochemical energy storage". In: *Applied Energy* 109 (2013), pp. 352–359. ISSN: 03062619. DOI: 10.1016/j.apenergy.2013.01.087.

[41] Mohamed A Mohamed, Andrew K Galwey & Samih A Halawy. "The activities of some metal oxides in promoting the thermal decomposition of potassium oxalate". In: *Thermochimica Acta* 387 (2002), pp. 63–74.

[42] A. Morales et al. "Enthalpies of formation and standard entropies for some potassium Tutton salts". In: *Chemical Thermodynamics and Thermal Analysis* 8 (2022), p. 100085. ISSN: 26673126. DOI: 10.1016/j.ctta.2022.100085.

[43] Mohau Moshoeshoe, Misael Silas Nadiye-Tabbiruka & Veronica Obuseng. "A Review of the Chemistry, Structure, Properties and Applications of Zeolites". In: *American Journal of Materials Science* 2017.5 (2017), pp. 196–221. DOI: 10.5923/j.materials.20170705.12.

[44] Kokouvi Edem N'Tsoukpoe et al. "A systematic multi-step screening of numerous salt hydrates for low temperature thermochemical energy storage". In: *Applied Energy* 124 (2014), pp. 1–16. ISSN: 03062619. DOI: 10.1016/j.apenergy.2014.02.053.

[45] Emmanuel Nyankson et al. "Synthesis and characterisation of zeolite-A and Zn Exchanged Zeolite-A based on Natural Aluminosilicates and their Potential Applications". In: *Cogent Engineering* 5.1 (2018). ISSN: 23311916. DOI: 10.1080/23311916.2018.1440480.

[46] Metso Outotec Finland Oy. *HSC Chemistry version 6.12*. 2007.

[47] Darren C. Peets et al. "Crystal Growth, Structure, and Noninteracting Quantum Spins in Cyanochroite, K2Cu(SO4)2·6H2O". In: *ACS Omega* 7.6 (2022), pp. 5139–5145. ISSN: 24701343. DOI: 10.1021/acsomega.1c06143.

[48] PubChem National Center for Biotechnology Information. *Zinc sulphate heptahydrate*. URL: https://pubchem.ncbi.nlm.nih.gov/compound/ZINC-sulfate-heptahydrate (visited on 03/08/2023).

[49] Ata Ur Rehman, Zheng Maosheng & Asif Hayat. "Hydration performance and cycling stability of three TCM: MgSO4, ZnSO4 and FeSO4". In: *International Journal of Energy Research* 44.8 (2020), pp. 6981–6990. ISSN: 1099114X. DOI: 10.1002/er.5470.

[50] Ata Ur Rehman et al. "Thermochemical heat storage ability of ZnSO4·7H2O as potential long-term heat storage material". In: *International Journal of Energy Research* 45.3 (2021), pp. 4746–4754. ISSN: 1099114X. DOI: 10.1002/er.6077.

[51] K Reisdorf & J Pannetier. "Dehydration Reactions of Gypsum: A Neutron and X-Ray Diffraction Study". In: *Journal of Solid State Chemistry* 85 (1990), pp. 23–30.

[52] Erwin Riedel & Christoph Janiak. "4 Die Elemente der Hauptgruppen". In: *Anorganische Chemie*. De Gruyter, 2022, pp. 407–706. DOI: 10.1515/9783110694444-004.

[53] Stefan Rönsch et al. "Zeolite Heat Storage: Key Parameters from Experimental Results with Binder-Free NaY". In: *Chemical Engineering and Technology* 43.12 (2020), pp. 2530–2537. ISSN: 15214125. DOI: 10.1002/ceat.202000342.

[54] Margarete Seeger et al. "Magnesium Compounds". In: *Ullmann's Encyclopedia of Industrial Chemistry*. Vol. 22. Weinheim, Germany: Wiley-VCH Verlag GmbH & Co. KGaA, 2012, pp. 41–77. DOI: 10.1002/14356007.a15{_}595.pub2.

[55] S G Sinha, N D Deshpande & D A Deshpande. "Dehydration of crystalline MnSO4* 4H2O". In: *Thermochimica Acta* 113 (1987), pp. 95–104.

[56] A. Souamti et al. "Synthesis, characterization and thermal analysis of K2M(SO4)2· 6H2O (M = Mg, Co, Cu)". In: *Journal of Thermal Analysis and Calorimetry* 122.2 (2015), pp. 929–936. ISSN: 15882926. DOI: 10.1007/s10973-015-4779-6.

[57] Jana Stengler, Inga Bürger & Marc Linder. "Thermodynamic and kinetic investigations of the SrBr2 hydration and dehydration reactions for thermochemical energy storage and heat transformation". In: *Applied Energy* 277 (2020). ISSN: 03062619. DOI: 10.1016/j.apenergy.2020.115432.

[58] Thermo Fisher Scientific. *Safety Data Sheet Magnesium bromide hexahydrate*. Tech. rep. 2021.

[59] Thermo Fisher Scientific Inc. *Manganese sulphate tetrahydrate*. URL: https://www.fishersci.de/shop/products/manganese-ii-sulfate-tetrahydrate-certified-ar-analysis-fisher-chemical/11462844 (visited on 02/03/2023).

[60] Thermo Fisher Scientific Inc. *Strontium bromide hexahydrate*. URL: https://www.thermofisher.com/order/catalog/product/B22553.22?SID=srch-hj-B22553.22 (visited on 02/03/2023).

[61] U.S. Energy Information Administration. "International Energy Outlook 2021 with projections to 2050". In: *International Enrgy Outlook Narrative* (2021).

[62] Holger Urs Rammelberg et al. "An optimization of salt hydrates for thermochemical heat storage". In: *International Symposium on Innovative Materials for processes in Enrgy Systems* (2013).

[63] V. M. Van Essen et al. "Characterization of MgSO4 hydrate for thermochemical seasonal heat storage". In: *Journal of Solar Energy Engineering, Transactions of the ASME* 131.4 (2009), pp. 1–7. ISSN: 01996231. DOI: 10.1115/1.4000275.

[64] Donald D. Wagman et al. *The NBS tables of chemical thermodynamic properties*. Vol. 11. Washington DC, USA: American Chemical Socienty, 1982, pp. 1–407.

[65] W W Wendlandt. "The thermal properties of inorganic compounds III. Strontium chloride 6-hydrate". In: *Thermochimica Acra* 12 (1975), pp. 359–366.

[66] Egon Wildermuth et al. "Iron Compounds". In: *Ullmann's Encyclopedia of Industrial Chemistry*. Vol. 20. Weinheim, Germany: Wiley-VCH Verlag GmbH & Co. KGaA, 2012, pp. 41–62. DOI: 10.1002/14356007.a14{_}591.

[67] Franz Wirsching. "Calcium Sulfate". In: *Ullmann's Encyclopedia of Industrial Chemistry*. Vol. 6. Weinheim, Germany: Wiley-VCH Verlag GmbH & Co. KGaA, 2012. DOI: 10.1002/14356007.a04{_}555.

Nomenclature

Acronyms

CAS no.	chemical substance identification number by the Chemical Abstracts Service
DSC	Differntial scanning calorimetry
ECHA	European Chemicals Agency
RT	Room temperature
TCES	Thermochemical energy storage
TGA	Thermogravimetric analysis

Subscripts

avg.	average
dehyd	dehydration
exp.	experimental
theo.	theoretical

Roman symbols

Δh°_m	energy storage density	kJ/kg
Δh°_R	standard reaction enthalpy	kJ/mol
Δh°_V	energy storage density	kJ/m^3
ν	stoichiometric coefficient	mol
ρ	density	g/cm^3
c_p	specific isobaric heat capacity	kJ/(kg K)
h°_f	standard formation enthalpy	kJ/mol
M	molare mass	g/mol
m	mass	kg
Q	heat	J
T	temperature	°C
V_c	volume condensed water	mL
V_s	stoichiometric volume	mL
X_i	conversion	

List of Figures

List of Tables